Variation of axial and oblique astigmatism with accommodation across the visual field

Tao Liu
School of Optometry, Indiana University, Bloomington, IN, USA ✉

Larry N. Thibos
School of Optometry, Indiana University, Bloomington, IN, USA 🏠 ✉

In this study we investigated the impact of accommodation on axial and oblique astigmatism along 12 meridians of the central 30° of visual field and explored the compensation of corneal first-surface astigmatism by the remainder of the eye's optical system. Our experimental evidence revealed no systematic effect of accommodation on either axial or oblique astigmatism for two adult populations (myopic and emmetropic eyes). Although a few subjects exhibited systematic changes in axial astigmatism during accommodation, the dioptric value of these changes was much smaller than the amount of accommodation. For most subjects, axial and oblique astigmatism of the whole eye are both less than for the cornea alone, which indicates a compensatory role for internal optics at all accommodative states in both central and peripheral vision. A new method for determining the eye's optical axis based on visual field maps of oblique astigmatism revealed that, on average, the optical axis is 4.8° temporal and 0.39° superior to the foveal line-of-sight in object space, which agrees with previous results obtained by different methodologies and implies that foveal astigmatism includes a small amount of oblique astigmatism (0.06 D on average). Customized optical models of each eye revealed that oblique astigmatism of the corneal first surface is negligible along the pupillary axis for emmetropic and myopic eyes. Individual variation in the eye's optical axis is due in part to misalignment of the corneal and internal components that is consistent with tilting of the crystalline lens relative to the pupillary axis.

Introduction

Astigmatism in optical systems, including the eye, has two principal causes. In rotationally symmetric optical systems, oblique astigmatism occurs for object points displaced from the optical axis of symmetry as described quantitatively by Coddington's equations for obliquely incident rays (Freeman & Hasler, 1999). The magnitude of oblique astigmatism increases with field angle, is independent of meridian, and has a radially oriented axis. If the system lacks rotational symmetry (e.g., because of toroidal refracting surfaces), astigmatism occurs even along the optical axial (where oblique astigmatism is zero by definition) due to variations of surface curvature for different meridians (Malacara, 2004; Rabbetts, 2007). Unlike oblique astigmatism, the magnitude and axis of axial astigmatism are independent of field angle. When astigmatism is represented by a power vector in Cartesian form (Thibos, Wheeler, & Horner, 1997), optical theory predicts that total astigmatism is the vector sum of these oblique and axial forms of astigmatism (Liu & Thibos, 2016). This suggests that decomposing total astigmatism into its axial and oblique components will lead to a clearer understanding of the nature of ocular astigmatism of the human eye and the influence of accommodation.

In human eyes, the variation of measured astigmatism across the visual field often exhibits temporal-nasal asymmetry (Lotmar & Lotmar, 1974; Millodot, 1981) and to a less extent superior-inferior asymmetry (Atchison, Pritchard, & Schmid, 2006). This asymmetry has been attributed to the misalignment (angle α) of the visual axis (connecting the fixation point, nodal point, and fovea) to the eye's optical axis, which suggests that astigmatism for foveal vision is typically a combination of axial and oblique astigmatisms. One aim of the present study was to test this prediction by measuring each component in isolation and in combination not only for the fovea but also for a significant portion of the central visual field.

When the eye accommodates to bring objects at various distances into focus, the shapes of the anterior and posterior surface of the crystalline lens change (Dubbelman, Van der Heijde, & Weeber, 2005;

Rosales, Dubbelman, Marcos, & van der Heijde, 2006) and refractive index distribution also changes significantly (Garner & Smith, 1997; Vazquez, Acosta, Smith, & Garner, 2006). These lenticular changes affect the eye's focusing power (López-Gil et al., 2013) and spherical aberration (Cheng et al., 2004) and so might reasonably be expected to affect either or both forms of astigmatism as well. This expectation is consistent with the well-known variation of foveal astigmatism with accommodation called *sectional astigmia* or *astigmatic accommodation* (Beck, 1965; Brzezinski, 1982; McFadden, 1925) but leaves open the question of which type of astigmatism is responsible. The available evidence suggests that axial astigmatism changes more than oblique astigmatism when the eye accommodates since foveal changes (Cheng et al., 2004; Millodot & Thibault, 1985; Radhakrishnan & Charman, 2007; Ukai & Ichihashi, 1991) are larger than changes in the near peripheral visual field (eccentricity <30°) (Calver, Radhakrishnan, Osuobeni, & O'Leary, 2007; Davies & Mallen, 2009; Lundström, Mira-Agudelo, & Artal, 2009; Mathur, Atchison, & Charman, 2009; Smith, Millodot, & McBrien, 1988; Whatham et al., 2009), although larger changes have been reported in the far periphery (Smith et al., 1988). To help resolve this issue, the present study monitored changes in the axial and oblique components of ocular astigmatism over a range of accommodative states.

Like any ocular aberration, astigmatism of either type of might be due to the cornea, the crystalline lens, or the alignment of these refracting elements with each other and the eye's pupil. Previous work has shown that astigmatism measured along the foveal line of sight (LoS) in the nonaccommodating eye is less than that of the cornea alone (Artal, Benito, & Tabernero, 2006; Artal & Guirao, 1998; Artal, Guirao, Berrio, & Williams, 2001; Kelly, Mihashi, & Howland, 2004; McKendrick & Brennan, 1996). This well-established result implies that astigmatism of the crystalline lens compensates partially for corneal astigmatism when accommodation is relaxed, as summarized clinically by Javal's Rule (Rabbetts, 2007). Whether astigmatism of the cornea and crystalline lens continue to balance each other along the LoS when the eye accommodates remains an open question. We might further ask if this aberration balancing is restricted to the axial or the oblique components of foveal astigmatism.

Previous investigations of the relative contributions of cornea and lens to measured astigmatism in peripheral vision are scarce. One early study compared the corneal astigmatism of aphakic eyes with ocular astigmatism of phakic eyes up to 40° eccentricity horizontally, and concluded that lenticular astigmatism augments rather than balances the cornea in peripheral vision (Millodot, 1984). However, the opposite conclusion was reached in a later and more rigorous study

(Atchison, 2004). Methodological issues might be partially responsible for this controversy since misalignment between measurement axes of corneal topographers (typically based on Purkinje images) and ocular astigmatism (typically along the foveal LoS, which is unrelated to Purkinje images) can lead to false conclusions if overlooked (Applegate, Thibos, Twa, & Sarver, 2009; Salmon & Thibos, 2002).

Given the limited understanding of ocular astigmatism reviewed above, we aimed to characterize axial and oblique components of ocular astigmatism across the central 30° of visual field and their variation with accommodation in emmetropic and myopic eyes. To achieve this goal required developing a new method for locating the optical axis from aberrometry data in order to resolve measured astigmatism into its axial and oblique components. We then determined the relative contributions of cornea and crystalline lens to these two components of astigmatism at each field location over a range of accommodation states.

Methods

Astigmatism analysis in this report was based on optical measurements obtained in our recently described study of wavefront aberrometry across the visual field in the accommodating eye (Liu, Sreenivasan, & Thibos, 2016). That study employed a custom-built scanning Shack-Hartmann aberrometer to measure the left eye's wavefront aberration over the central 30° of visual field in 34 normal, healthy subjects (16 emmetropic and 18 myopic). One emmetropic subject was excluded from analysis because of data corruption by a partially closed upper eyelid. All measurements were obtained without the use of cycloplegic drugs. Additional methods not previously described in (Liu et al., 2016) are summarized below.

Ocular aberration measurement

A custom-built instrument (X. Wei & L. Thibos, 2010a) (Indiana Scanning Aberrometer for Wavefronts, I SAW) was used to measure ocular aberrations at 850 nm over a 30° diameter field of view centered on the foveal line-of-sight. Measurements were obtained for a randomized sequence of 37 locations (eccentricities 0°, 5°, 10°, 13.5° along 12 visual meridians 0° to 360° in 30° steps) in 16 s. (Liu et al., 2016). Normal blinking was permitted, with subsequent rejection of corrupt data images by quality control procedures. This sequence was repeated for eight levels of accommodative demand ranging from 1 D beyond the far point to 6 D in front of the far point, in 1 D steps.

Wavefront slope data were fit with derivatives of Zernike polynomials over the circumscribed circular domain of the natural pupil, which takes into account the pupil's elliptical appearance when viewed obliquely (Wei & Thibos, 2010b).

The pupil coordinate system and nomenclature for reporting Zernike coefficients conformed to ANSI standard Z80.28 (ANSI, 2010), with the z axis coinciding with the peripheral LoS and the measurement axis of the aberrometer. From the Zernike coefficients for astigmatism (C_2^2, C_2^{-2}) for the natural pupil size we computed dioptric power vectors $\mathbf{J} = (J_0, J_{45})$ in Cartesian form according to Equation 1

$$\begin{cases} J_0 = \dfrac{2\sqrt{6}C_2^2}{R^2} \\ J_{45} = \dfrac{2\sqrt{6}C_2^{-2}}{R^2} \end{cases} \quad (1)$$

where R is the radius of the natural pupil in mm. The conversion from Cartesian to polar form is given by Equation 2

$$\begin{cases} J = \sqrt{J_0^2 + J_{45}^2} \\ \phi = \tan^{-1}(J_{45}/J_0)/2 \end{cases} \quad (2)$$

where J is the magnitude of astigmatism (half of the cylinder power) and ϕ (the meridian of maximum positive power) is the axis of astigmatism. In this report we refer to a collection of power vectors obtained from the 37 aberrometer locations as a visual field map of the astigmatic vector $\mathbf{J}$. Graphical conventions for displaying visual field maps of astigmatism are described in the Appendix (Figure A1). Unlike clinical conventions, astigmatism in this report refers to the eye (not the lens used to correct the eye) as recommended by ANSI standard Z80.28 (ANSI, 2010). This explains why Zernike coefficients and power vector values have the same sign in Equation 1. For example, a positive value of J_0 in this report indicates "against-the-rule" astigmatism in clinical terminology.

Corneal topography and anterior chamber depth

Videokerotography was measured using the Medmont corneal topographer (E300 version 4.12, Medmont International Pty, Ltd., Victoria, Australia) with the measurement axis containing the fixation point and normal to the cornea (commonly called the VK axis). We assumed corneal astigmatism is invariant with accommodation (He, Gwiazda, Thorn, Held, & Huang, 2003) and therefore took no special precautions to control accommodative state during corneal topography or Lenstar measurements of anterior chamber depth. We verified this assumption under the conditions of our experiment for one subject under normal and cyclopleged conditions and found negligible differences. The difference in corneal axial astigmatism was 0.03 D, and the difference in the regression coefficient of corneal oblique astigmatism was 0.03×10^{-3} D/deg^2. We presume the measurements were obtained for a relaxed eye because the fixation target in both instruments is a poor stimulus for accommodation (flashing red light for Lenstar and black disk for Medmont).

Corneal elevation data were fit by the method of least-squares to a rotationally symmetric conic surface with conic constant p ($p = 1$ is a circle, with other positive p values being ellipses, and $p < 0$ are hyperbolas; Rabbetts, 2007) and curvature c (first term in Equation 3). By subtracting the conic surface from the elevation map, the residual shape (second term in Equation 3) was then fit with Zernike polynomials up to the 6th order (Schwiegerling, Greivenkamp, & Miller, 1995) for the corneal diameter ($D = 2R_C$, where R_C is the measured corneal radius) reported by the topographer. For optical modeling purposes the elevation height map was then expressed in polar coordinates by

$$z(r, \theta) = \frac{cr^2}{1 + \sqrt{1 - pc^2r^2}} + \sum_{i=1}^{36} C_i Z_i(\rho, \theta) \quad (3)$$

where z is the corneal height in mm, p is the unitless conic constant, c is curvature in mm^{-1}, C_i is ith Zernike coefficient in mm, Z_i is ith Zernike polynomial, r is radial distance from corneal apex (the intersection of measurement axis and cornea) in mm, θ is the meridional angle in radians, and $\rho = r / R_C$ is the normalized radial coordinate of points on the corneal surface.

Anterior chamber depth (defined as the distance from anterior surface of the cornea to anterior surface of the crystalline lens) was determined along the foveal LoS using Lenstar LS 900 (Haag-Streit AG, Koeniz, Switzerland), a partial coherence interferometer that reports corneal position, anterior chamber and lens thickness respectively (Suheimat, Verkicharla, Mallen, Rozema, & Atchison, 2015). Subjects were instructed to fixate the internal target (a flashing red dot) to control eye position and accommodative state. Lenstar data were not available for some subjects: in which case we assumed the average anterior chamber depth value (3.64 ± 0.55mm) of 33 normal eyes in our database.

Calculation of corneal anterior-surface aberrations from topography

Corneal topography was measured along a single measurement axis (the VK axis) but ocular aberrations

were measured along 37 different measurement axes (foveal plus 36 peripheral LoS). Therefore, in order to determine the contribution of the corneal first-surface to the measured aberrations, we used the optical design software program Zemax OpticStudio (Zemax, LLC, Kirkland, WA) to construct a customized optical model of each subject's eye based on corneal topography and Lenstar biometry. The details of this procedure are given in the Appendix. Ray tracing through these models provided wavefront aberration maps relative to the foveal LoS and each of the 36 peripheral LoS used experimentally.

Calculation of internal aberrations

In this report, *internal aberrations* refer to those ocular aberrations not accounted for by refraction at the anterior surface of the cornea. According to this definition, refraction by the posterior corneal surface, propagation of aberrated wavefronts through the anterior chamber (Roselló, Thibos, & Micó, 2014), and intrinsic lens aberrations are all factors that contribute to internal aberrations. No attempt was made to separately quantify these contributing factors. Since ocular and corneal aberrations were both specified in the entrance pupil plane for the same pupil diameter and referenced to a common axis (LoS) by the method described in the Appendix, internal aberrations could be computed for each state of accommodation by a vector subtraction of corneal first-surface aberrations (determined by ray tracing through customized optical models) from whole-eye aberrations (determined by empirical aberrometry) at each point in the visual field. For reporting purposes, computed Zernike coefficients (i.e., RMS wavefront error in microns) for internal astigmatism were converted by Equation 1 to a power vector description in diopters. To further decompose ocular, corneal first-surface, or internal astigmatism into axial and oblique subtypes required an appropriate definition and method for locating the optical axis as described next.

Locating the optical axis

The optical axis is an important reference for this study because it locates the direction in visual space along which oblique astigmatism is zero. For a rotationally symmetric system, the optical axis is usually taken to be the line connecting centers of curvatures of the optical elements comprising the system. For systems lacking rational symmetry, such as the eye, a regression line fit to the curvature centers may be adequate for many applications. Theoretically, in situations where a paraxial approximation of the system is sufficient, the optical axis may be defined as the path of collinear entrance and exit rays (Harris,

2009). For present purposes, however, the most useful definition is a line passing through the eye's entrance pupil that is coincident with the axis of rotational symmetry for the oblique component of ocular astigmatism (Liu & Thibos, 2016).

To locate the optical axis from aberrometry measurements, we used a novel, iterative method illustrated in the Appendix. We refer to the angular separation between this optical axis and the foveal LoS as angle alpha-prime (α'). Unlike the traditional angle alpha (between the eye's optical and visual axes, which doesn't exist if the optical axis is skew to the visual axis), angle α' will always exist because the LoS and optical axis (by our definition) intersect at the center of the entrance pupil.

Resolution of astigmatism into its axial and oblique components

According to the definition adopted above, a chief ray aligned with the optical axis experiences zero oblique astigmatism and therefore the trace of that chief ray locates the optical axis. However, if toric refracting surfaces are present, then ocular astigmatism may still be nonzero along the optical axis because of axial astigmatism. We take advantage of that fact to define the system's axial astigmatism as that value of ocular astigmatism found (usually by interpolation) on the optical axis. We then computed a visual field map of oblique astigmatism $\mathbf{J}_{oblique}$ by performing a power vector subtraction (Liu & Thibos, 2016) of axial astigmatism $\mathbf{J}_{axial}$ from total astigmatism $\mathbf{J}_{total}$ for every field location,

$$\mathbf{J}_{oblique} = \mathbf{J}_{total} - \mathbf{J}_{axial} \quad (4)$$

using the same vector equation, ocular, corneal and internal astigmatisms were computed from Zernike aberration coefficients and then decomposed into axial and oblique component for evaluation.

According to optical theory (Welford, 1986), oblique astigmatism varies quadratically with eccentricity. Accordingly, we summarized the empirical field maps of oblique astigmatism by pooling the magnitude of oblique astigmatism J (diopters) across meridians for fitting with the quadratic Equation 5

$$J = \sigma \varepsilon^2 \quad (5)$$

where ε is the radial eccentricity (degrees from the optical axis) and σ is regression coefficient (Diopters/deg^2).

Results

In this section we organize the description of results into three broad categories of *ocular* (i.e., the whole eye,
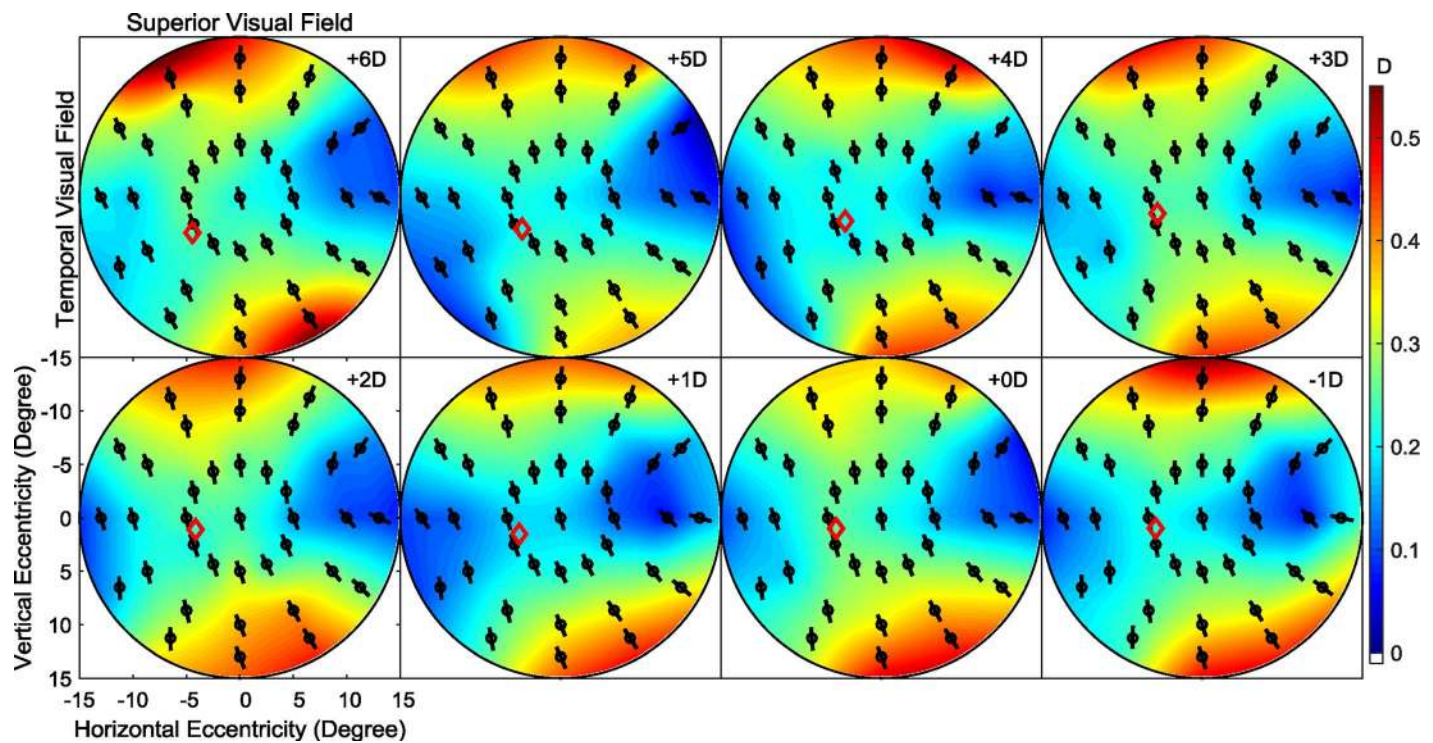
Figure 1. Ocular astigmatism maps of the central visual field for eight levels of accommodative demand for a typical individual (RH). Each map shows how measured ocular astigmatism varies across the central 30° diameter visual field (i.e., maximum eccentricity $\varepsilon =$ 15°). Field maps follow the conventions of Figure A1 (e.g., coordinate center of the visual field map is the foveal line-of-sight, with temporal visual field on the left and superior visual field on top). Black circles show the test locations, which are interpolated to make a continuous map with scale shown by the color bar on the far right. The short line through each symbol indicates the axis of astigmatism (i.e., the meridian of most positive power). The diamond symbols indicate the optical axis, as estimated from the visual field map using the method of Figure A2. Number in upper right corner of each map is nominal accommodative demand. The similarity of all eight maps indicates astigmatism is largely invariant to accommodation in this (and other) subjects.

as measured by aberrometry), *corneal* (as measured by videokeratography), and *internal astigmatism* (computed by subtracting corneal from total) representing the remainder of ocular astigmatism not accounted for by refraction at the anterior corneal surface. Within each of these three categories, we decompose the *total* astigmatism into *axial* and *oblique* components using Methods Equation 4. This organized collection of results is described first for a typical subject (RH) to demonstrate how the sequence of optical analysis proceeds for an individual eye. We then present population results to show trends and individual variability within and between populations of emmetropic and myopic eyes.

Ocular astigmatism

Total

Our main empirical finding is that the visual field map of ocular astigmatism for an individual eye is almost invariant with accommodation, as illustrated for a typical subject RH (emmetropic eye) in Figure 1.

Although the color maps show a degree of symmetry, the center of that symmetry is displaced from the coordinate origin (i.e., the LoS), which suggests this eye's optical system was not concentric with the LoS, and therefore foveal astigmatism is a combination of axial and oblique astigmatism. Applying our iterative method for locating the optical axis, the result for this subject (indicated by the red diamond) was about 4° temporal and 2° inferior to the LoS regardless of accommodative state (mean = 4°, SD = 0.37° horizontally; mean = 1.8°, SD = 0.92° vertically). By definition, oblique astigmatism is zero at the optical axis and therefore the interpolated astigmatism at the mean optical axis location is our best estimate of axial astigmatism.

The rotationally asymmetric patterns of total astigmatism magnitude (bow-tie centered on the estimated optical axis) in Figure 1 is expected theoretically when oblique astigmatism interacts with axial astigmatism (Liu & Thibos, 2016). In this case, theory predicts total astigmatism maps with two null points along the meridian perpendicular to the axial astigmatism axis. These null points result from the cancellation of
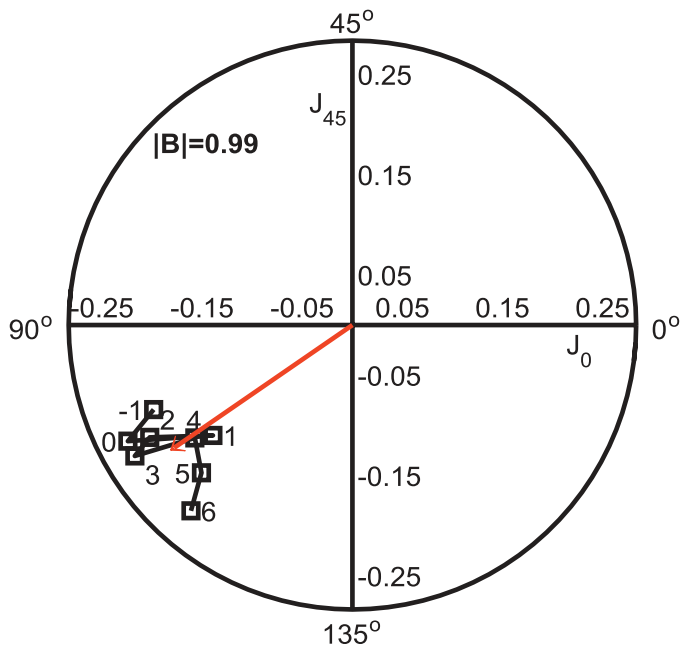
Figure 2. Variation of axial astigmatism (refers to the eye, opposite sign to clinical convention) with accommodation, as traced by the trajectory of two-dimensional power vectors. Symbols show the tip of the astigmatism power vector for accommodation demand indicated by adjacent numbers (subject RH). The x and y axis are the elements of the power vector J_0, J_{45}, respectively. As indicated by text Equation 2, the radial distance of each symbol from the origin equals the magnitude of astigmatism and the polar angle of symbol is double the axis of astigmatism. Connecting symbols in sequence with lines reveals the trajectory of axial astigmatism as the eye accommodates. Red arrow is the mean power vector across accommodative states for the axial component of astigmatism. Concentration parameter $|\mathbf{B}|$ is high (0.99) for these data, which indicates accommodation produces little variation from the mean.

oblique astigmatism by axial astigmatism. The opposite effect occurs in the meridian parallel to the axial astigmatism axis because axial astigmatism reinforces oblique astigmatism.

Axial

For this subject, the best estimate of axial astigmatism exhibited negligible changes during accommodation (J_0 mean $= -0.18$, $SD = 0.03$ D; J_{45} mean $= -0.12$, $SD = 0.03$ D) and clustered together with high concentration factor ($|\mathbf{B}| = 0.99$) about the mean (indicated by the red arrow) in the scatter map of Figure 2. For this subject the mean magnitude of axial astigmatism at the optical axis was 0.22 D axis 107° with negligible fluctuation over the 6 D range of accommodative demand. Inspecting the trace of axial astigmatism as this subject accommodated showed no

systematic changes. Assuming accommodation has no effect on corneal astigmatism, we infer from this result that differences in restraining forces on the crystalline lens resulting from ciliary muscle action were symmetrically exerted without changing surface toricity, tilt, or displacement in this eye.

Oblique

The oblique astigmatism component of each visual field map in Figure 1 was computed by subtracting axial astigmatism (a vector difference) from total astigmatism. Not surprisingly, since axial astigmatism in this eye was nearly constant for all accommodative states, the resulting field maps of oblique astigmatism were nearly identical for all accommodative states. Therefore, we averaged across accommodative states to produce the mean oblique astigmatism map shown in the upper panel of Figure 3. This mean map displays the expected rotational symmetry in magnitude, radial orientation of axis, and unique null point at zero eccentricity relative to the optical axis that are the traits of oblique astigmatism. The corresponding map of standard deviations of the eight states of accommodation is featureless and nearly zero in magnitude, indicating the substantial changes in lenticular shape associated with accommodation had little impact on ocular oblique astigmatism. Oblique astigmatism varied little (less than 0.05 D SD for any field location) as this subject accommodated to 6 D target. Pooling the mean map across meridians led to a fitted quadratic coefficient σ for the averaged oblique astigmatism $= 1.07 \times 10^{-3}$ D/deg^2, which corresponds to approximately $J = 0.24$ D oblique astigmatism at 15° eccentricity.

Population trends: Ocular astigmatism

Results shown in Figures 1 through 3 were for an individual eye. Corresponding results were obtained for all subjects and then averaged to observe population trends as shown in Figures 4 through 6. The upper panel of Figure 4 compares the average axial astigmatism for our emmetropic and myopic study populations. Only the left side of the graph is shown because both populations demonstrated consistent with-the-rule axial astigmatism ($J_0 < 0$). Comparing the relaxed state (accommodation demand 0 D) with the most accommodated state (accommodation demand 6 D), reveals that both populations tended to shift slightly towards against-the-rule astigmatism when focusing on near targets. However, the lack of a systematic trend between the limits of 0 and 6 D accommodation suggests that neither population exhibited a definitive variation as the eye accommodated. To verify this
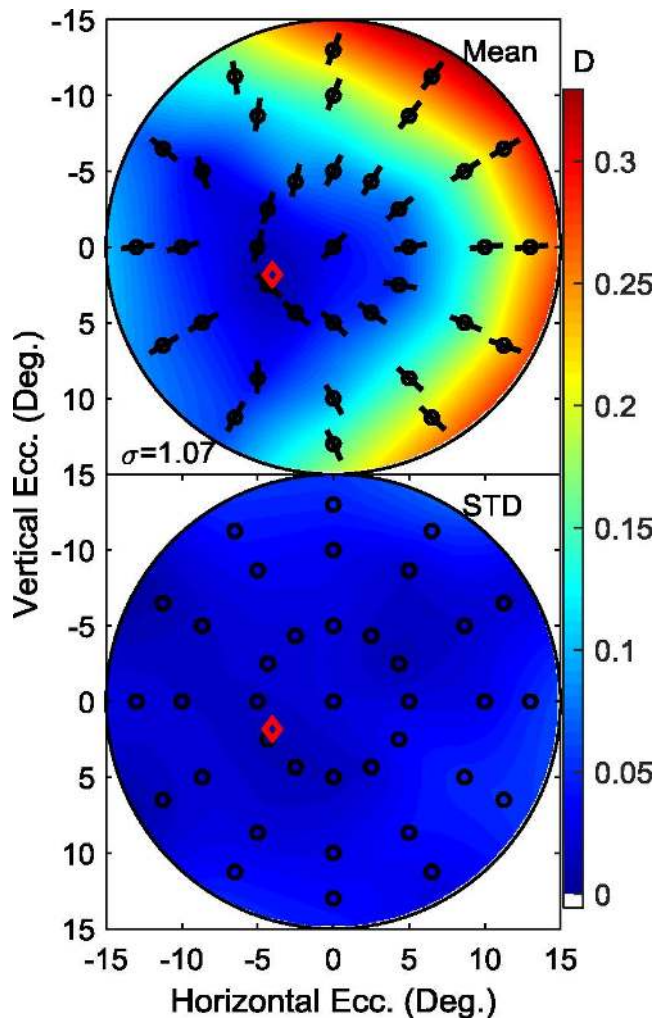
Figure 3. Ocular oblique astigmatism in the central visual field (subject RH). Top panel shows averaged oblique astigmatism across eight accommodative states. Color bar scale shows the magnitude of oblique astigmatism at each point in the visual field. Graphical conventions are the same as in Figure 1. Number in lower left corner is the quadratic coefficient σ in 10^{-3} D/deg^2 calculated by text Equation 5. Bottom panel shows standard deviation of oblique astigmatism across eight accommodative states for the same subject. Radial orientation of short black lines relative to the optical axis (red diamond) provides a visual confirmation that the method of Figure A2 accurately locates the eye's optical axis.
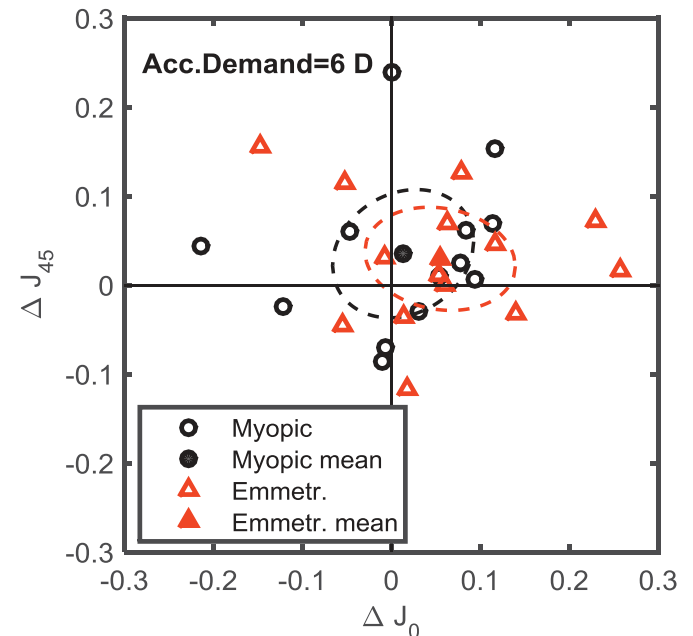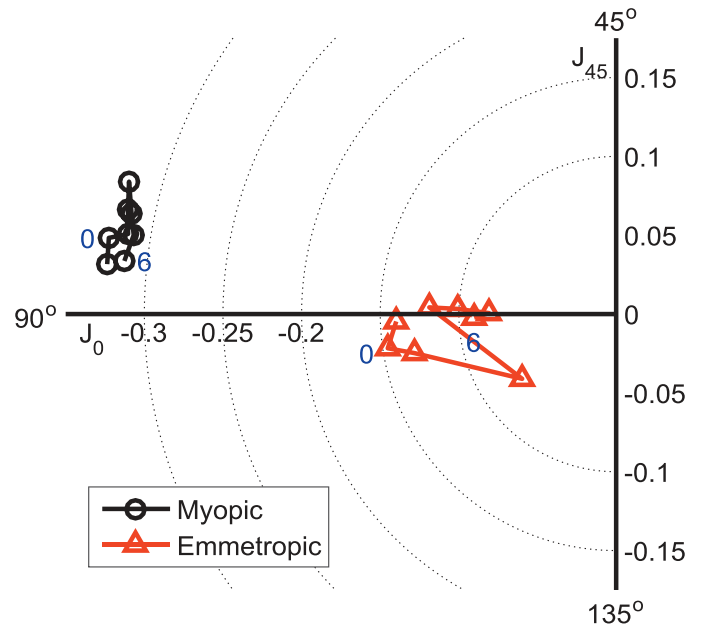
$\longrightarrow$

Figure 4. Comparison of effect of accommodation on axial astigmatism (refers to the eye, opposite sign to clinical convention) for emmetropic and myopic eyes. In top panel, symbols show the trajectory of the population mean of axial astigmatism as accommodation changes. As in Figure 2, numbers near selected symbols indicate accommodative demand. Since both population shows negative J_0 bias (with-

the-rule), only left half of the power vector space is displayed. Bottom panel shows change in axial astigmatism produced by maximum accommodation (6 D) from the resting state. The abscissa is J_0 component of accommodative astigmatism, equal to $J_0^{acc} - J_0^{relax}$, and the ordinate is the J_{45} component. Black and red symbols show individual variability of the two populations. The filled symbols are the mean of each population, and the 95% confidence ellipses for the two means are shown by dashed lines. Five myopic and one emmetropic subjects were excluded because instability of these eyes prevented valid wavefront measurements for 6 D accommodative demand.
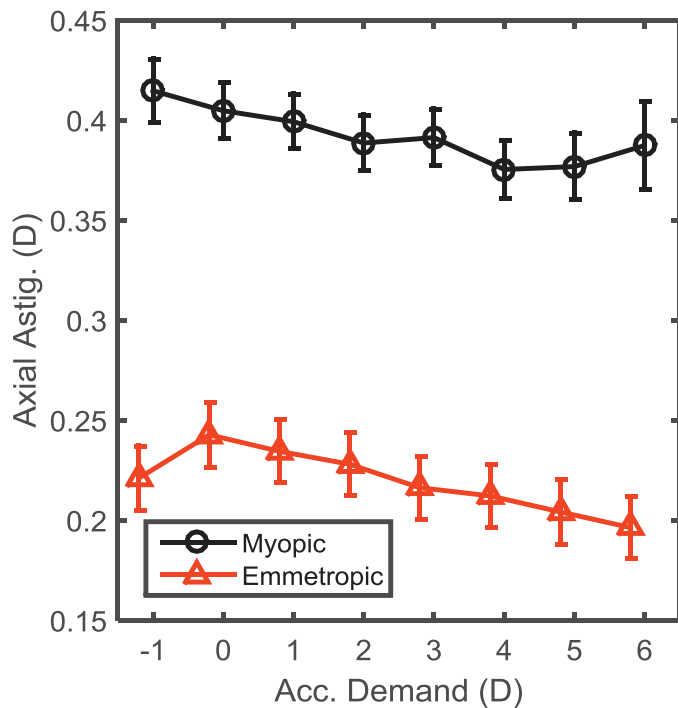
$\longleftarrow$

Figure 5. Comparison of variation of axial astigmatism magnitude with accommodation demand for emmetropic and myopic eyes. Symbols show the mean of axial astigmatism magnitude over all subjects in each population, and error bars show ±1 standard error of the mean (*SEM*). Abscissa values are staggered for clarity.
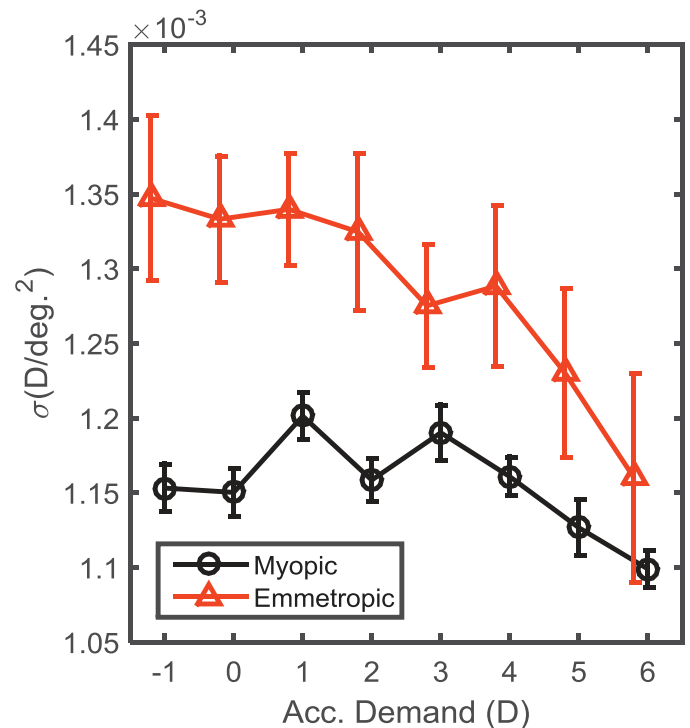

Figure 6. Comparison of variation of oblique astigmatism with accommodation demand for emmetropic and myopic eyes. Symbols show the mean of quadratic coefficients over all subjects in each population and error bars show ±1 standard error of the mean (*SEM*). Abscissa values are staggered for clarity.

observation, the power vector of accommodative axial astigmatism obtained by subtracting axial astigmatism of the relaxed state from the axial astigmatism of the most accommodated state is shown in the lower panel of Figure 4. Most noticeable from this graph is the relatively small difference in population means (filled symbols) compared to the larger intersubject variability in both populations. In addition, the coordinate origin (which corresponding to relaxed state) falls within the 95% confidence ellipses (dashed lines) of mean accommodative astigmatism, suggesting that the null hypothesis that accommodation has no effect on axial astigmatism cannot be rejected (Thibos et al., 1997).

Figure 5 compares the myopic and emmetropic population averages (a scalar calculation) of axial astigmatism magnitude at different level of accommodative demand. For both populations, the mean axial astigmatism magnitude slightly decreased as the eye accommodated, but these changes are of the same order of magnitude as individual variation within each population. At each level of accommodative demand, the two populations differed by about 0.2 D, which is in good agreement with the distance between the two clusters in the upper panel of Figure 4. The slight decrease (0.05 D) in mean axial astigmatism for emmetropes when the visual target was moved 1 D

beyond foveal far point is probably due to the inappropriate accommodation observed in these same individuals (Liu et al., 2016) as the eye returns to a positive resting state of accommodation for negative values of accommodative demand (Hennessy, 1975).

Population statistics for the oblique component of astigmatism were determined for our emmetropic and myopic groups by fitting each subject's data with the quadratic function of Equation 5 to obtain regression parameter σ that quantifies the rate of change of oblique astigmatism with visual field eccentricity relative to the optical axis. The population mean of this regression coefficient declined slightly with accommodation, more for emmetropic eyes than for myopic eyes as plotted in Figure 6. Emmetropic eyes showed more individual variability than myopic eyes. At 15° eccentricity, the difference in oblique astigmatism between the most relaxed and most accommodative state was 0.04 D for emmetropic eyes and 0.01 D for myopic eyes. Although the emmetropic population exhibited more oblique astigmatism than myopic eyes at all accommodative states, the maximum difference between populations was only 0.04 D at 15° eccentricity. Along the LoS (approximately 5° from the optical axis), about 0.06 D oblique astigmatism was present for both groups.

Corneal astigmatism

Total

Corneal topography was measured with accommodation relaxed, and we assumed the aberrations computed from topography applied also to other states of accommodation (He et al., 2003). Figure 7 shows the total (upper panel) and oblique astigmatism (lower panel) calculated from corneal topography data for subject RH across the central 30° visual field. Like the total ocular astigmatism map shown in Figure 1, the colored map of total corneal astigmatism in Figure 7 exhibited a bow-tie pattern indicative of the interaction between axial and oblique astigmatism.

Axial

Corneal axial astigmatism (0.81 D axis 91°) for subject RH dominated oblique astigmatism to such an extent that a null point indicating balancing of these two aberrations did not occur within the central 30° of visual field. This result is evident also in the parallel orientation of lines drawn through each symbol indicating axis of astigmatism at each field location.

Oblique

Oblique astigmatism of the cornea ($\sigma = 1.50 \times 10^{-3}$ D/deg^2) was greater than that of the whole eye (1.07×10^{-3} D/deg^2), indicative of compensation by internal optics. This compensation is rather complicated to compute, however, since the local optical axis of the cornea (cross symbol) deviated from optical axis of the whole eye (diamond symbol) about 2.8° for subject RH. This implies that the optical axes of cornea and lens are not collinear for this subject, which was true also for other subjects.

Internal astigmatism

Total

By subtracting corneal astigmatism from ocular astigmatism, the internal astigmatism was revealed (Figure 8, upper panel) for subject RH averaged across states of accommodation. We display only the average maps because the spatial patterns of magnitude (color map) and axes (oriented symbols) were nearly identical for all accommodative states, indicating that the total internal astigmatism is invariant with accommodation despite large changes in the shape and gradient index distribution of the crystalline lens. This result is not unexpected given the results of Figure 1, and our assumption that corneal astigmatism is unaffected by accommodation.
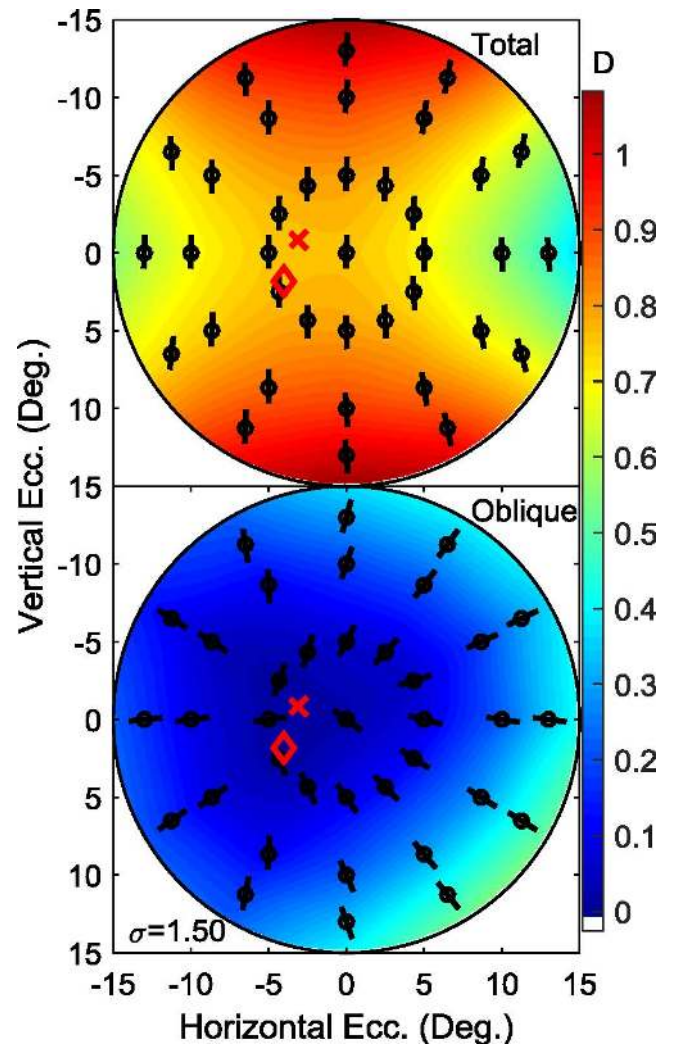

Figure 7. Corneal astigmatism of individual RH. Top panel is a visual field map of corneal total astigmatism. Bottom panel shows the oblique astigmatism component of the upper map. Number in the lower left corner is quadratic coefficient σ in 10^{-3} D/deg^2. Graphical conventions are the same as in Figure 1. The diamond symbols indicate the optical axis of the whole eye, while cross symbols indicate the optical axis of the cornea. Upper and lower panels have very different patterns of axis (shown by orientation of short lines through symbols), indicating that total corneal astigmatism is dominated by axial astigmatism in this eye.

Axial

The average across accommodative states of the magnitude of internal axial astigmatism was 0.58 D, which is about two thirds of corneal axial astigmatism. The axis of internal axial astigmatism was nearly horizontal (175°) in this eye, which prevailed against the oblique contribution (lower panel of Figure 7) in the central 30° visual field. This explains why the axis of total internal astigmatism is nearly uniformly orientated horizontally everywhere in the measured visual
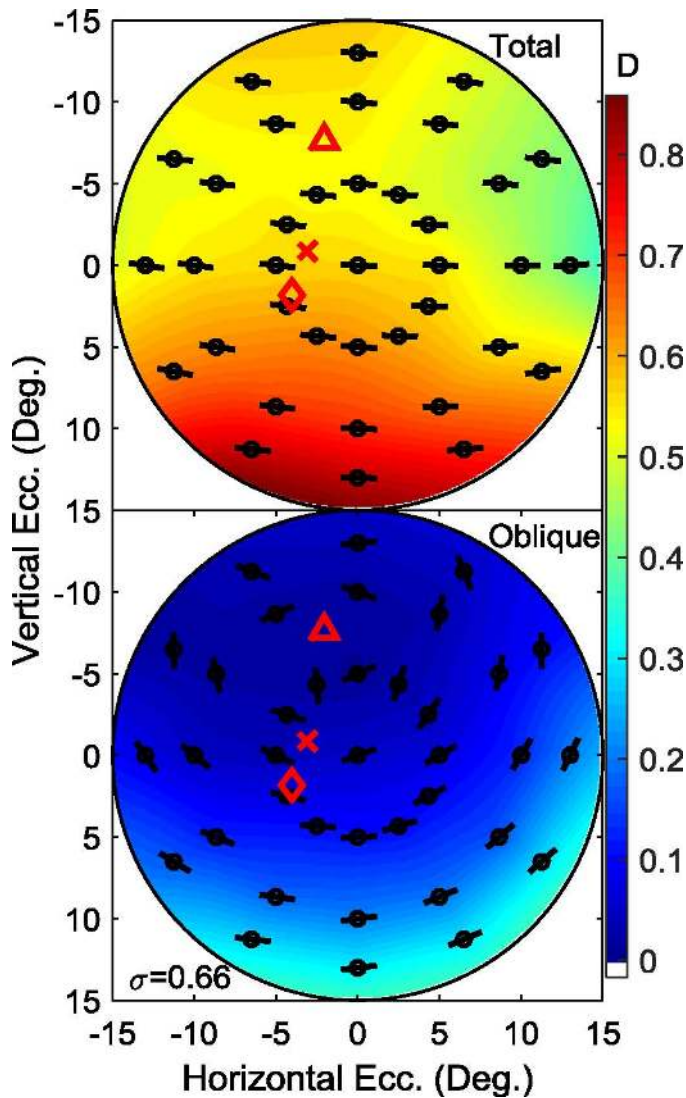
Figure 8. Internal astigmatism of individual RH. Top panel shows the total astigmatism map of internal optics averaged across eight levels of accommodative state. Bottom panel shows internal oblique astigmatism (averaged across eight accommodative states) is tangentially oriented, unlike the radial pattern seen in cornea (Figure 7). Number in the lower left corner is quadratic coefficient σ in 10^{-3} D/deg^2. Graphical conventions are the same as in Figure 1. The diamond symbols indicate the optical axis of the whole eye, cross symbols indicate the optical axis of cornea, and triangle symbols represent the optical axis of internal optics. Upper and lower panels have very different patterns of axis (shown by orientation of short lines through symbols), indicating that total internal astigmatism is dominated by axial internal astigmatism in this eye.

field (upper panel of Figure 8). Notice that this horizontal axis of total internal astigmatism is perpendicular to the vertical axis of total corneal axial astigmatism for this subject (Figure 7, top panel). This means that corneal astigmatism is compensated by internal astigmatism in both magnitude and axis.

Unlike the corneal axial astigmatism of this eye, for which axial astigmatism reinforced oblique astigmatism along the (vertical) axis of axial astigmatism, the internal axial astigmatism reinforced oblique internal astigmatism perpendicular to the (horizontal) axis of axial astigmatism. This difference in behavior can be traced to the conventional pattern of radial axes of oblique astigmatism of the cornea compared to the unconventional pattern of tangential axes of oblique astigmatism internally.

Oblique

Inspection of the field map for subject RH's internal oblique astigmatism (Figure 8, bottom panel) reveals several surprising features. Although the magnitude of internal oblique astigmatism (color map) shows the expected rotational symmetry about the local optical axis of the internal component (triangle symbol), the axes of internal oblique astigmatism (oriented line symbols) indicate obvious tangential orientation instead of the expected radial orientation observed from ocular and corneal oblique astigmatism (Figures 3 and 7). These tangentially orientated axes indicate that the net impact of internal optics (i.e., intrinsic astigmatism of the crystalline lens, propagation of astigmatic wavefronts, and refraction by posterior cornea) is yielding more refractive power in the sagittal than in the tangential meridians, which is the opposite of textbook descriptions of the effect of oblique astigmatism on image formation. (This unusual behavior is elaborated in Discussion.) As a result, corneal oblique astigmatism was mitigated by internal oblique astigmatism. Quantitatively, internal oblique astigmatism ($\sigma = 0.66 \times 10^{-3}$ D/deg^2) reduced corneal oblique astigmatism ($\sigma = 1.50 \times 10^{-3}$ D/deg^2) roughly by one third, resulting in an intermediate level of ocular oblique astigmatism ($\sigma = 1.07 \times 10^{-3}$ D/deg^2). However, unlike total astigmatism, the quadratic coefficients of oblique astigmatism cannot be added linearly in principle because they are referenced to local optical axes that are not aligned with each other. For RH, the local optical axis of the lens (triangle symbol) is superior to the corneal axis (cross symbol), and the angle between them is 6.86°. This misalignment explains the deviation of the ocular optical axis from either of the local optical axes.

Population trends: Compensation of corneal by internal astigmatism

Axial

The analysis described in the preceding section showed for one subject (RH) how the magnitude of corneal axial astigmatism is modulated by the internal

axial astigmatism. Perhaps surprisingly, the internal component was found to be invariant with accommodation so we wished to know if this is true for other eyes as well. Internal axial astigmatism had a horizontal axis in subject RH, which was perpendicular to the vertical axis for corneal axial astigmatism, restated in terms of power vectors, $J_0 < 0$ for the cornea but $J_0 > 0$ internally. This change in sign makes it clear why their sum (i.e., ocular axial astigmatism) is less than the corneal contribution, which we summarize by terms such as "compensation" or "balancing." In general, the axes of corneal and internal astigmatism are not necessarily orthogonal, so a vector sum must be computed to assess the effect of their interaction on the magnitude and axis of ocular astigmatism for other eyes in the study population.

For each subject in our emmetropic population, the power vectors for the two components (corneal and internal) of axial astigmatism and their vector sum (ocular) were averaged over accommodation states for graphical display in Figure 9 (one panel for each subject). For the majority of the emmetropic eyes, corneal (blue arrow) and internal (black arrow) axial astigmatism vectors are roughly aligned but in opposite directions, which implies their J_0 components have opposite signs, their J_{45} components have opposite signs, and their astigmatic axes are orthogonal. These results confirm that subject RH is typical of the other emmetropic subjects in our study population, as well as the myopic population as shown in Figure 10. Thus, we are led to conclude that at least partial balancing of corneal axial astigmatism by internal axial astigmatism is commonplace, in the spirit of Javal's Rule of clinical optometry and ophthalmology, for all states of accommodation.

Exceptions to the balancing trend do occur. For example, emmetropic subject EJ exhibited negligible internal axial astigmatism, so ocular axial astigmatism was due entirely to the cornea in this eye. For two other emmetropic subjects (BA and CM) the angle between the corneal and internal power vectors was nearly 90° rather than 180°, and therefore their vector sum is greater than either one alone in magnitude with direction different from either corneal or internal directions. One unusual myopic subject is DK, who was free of corneal axial astigmatism. Thus ocular axial astigmatism was due entirely to the internal component in that subject.

Oblique

The preceding analysis of axial astigmatism raises the corresponding question of whether corneal oblique astigmatism might be balanced to some degree by internal oblique astigmatism. We pursued this question quantitatively by defining the quantity "Corneal to Ocular Change" (COC) as a measure of how effectively oblique astigmatism of the corneal first surface is reduced by internal oblique astigmatism as quantified by the quadratic fit coefficients σ used to summarize oblique astigmatism across visual field. Since these coefficients were nearly independent of accommodative demand, we averaged them across accommodative states before computing COC for each subject as a percentage according to Equation 6

$$\text{COC} = \frac{\sigma_{\text{ocular}} - \sigma_{\text{corneal}}}{\sigma_{\text{corneal}}} \times 100 \quad (6)$$

Negative values of COC indicate compensation, whereas positive values indicate reinforcement. For emmetropic eyes the population mean was −19% and for myopic eyes was −17%. These two means were not significantly different ($p = 0.67$, t test), which justifies pooling across populations to show frequency histogram of COC for all 33 subjects in Figure 11. Most eyes showed significant compensation, with only two of 33 eyes exhibiting reinforcement. From these data we conclude that oblique astigmatism of the hypothetical average adult eye is 18% less than that of the cornea because of compensation by internal optics.

Ocular

As shown above, both axial and oblique components of corneal astigmatism were balanced by internal optics, thereby reducing astigmatism of the whole eye for all states of accommodation. However, one emmetropic subject (SL) and two myopic subjects (OS, DK) demonstrated systematic variation of axial astigmatism with accommodation as shown for one eye in Figure 12. As accommodative demand increased, the axial component of internal astigmatism (black triangles) increased in magnitude, but its axis (indicated by small lines through symbols) remained perpendicular to the corneal axis (blue squares and lines). Because these two components had orthogonal axes (hence, their power vectors had opposite signs), when summed, the magnitude of ocular axial astigmatism (red diamonds) declined with accommodation as the internal component increased. This resolution of seemingly paradoxical behavior provides a compelling example of the importance of treating astigmatism as a vector quantity when analyzing the interaction of various components of a multi-element system such as the eye.

Population trends: Relative alignment of cornea and internal optics

Our novel method for locating the visual field direction of the optical axis from aberrometry allows a comparison to be drawn in Figure 13 between our two
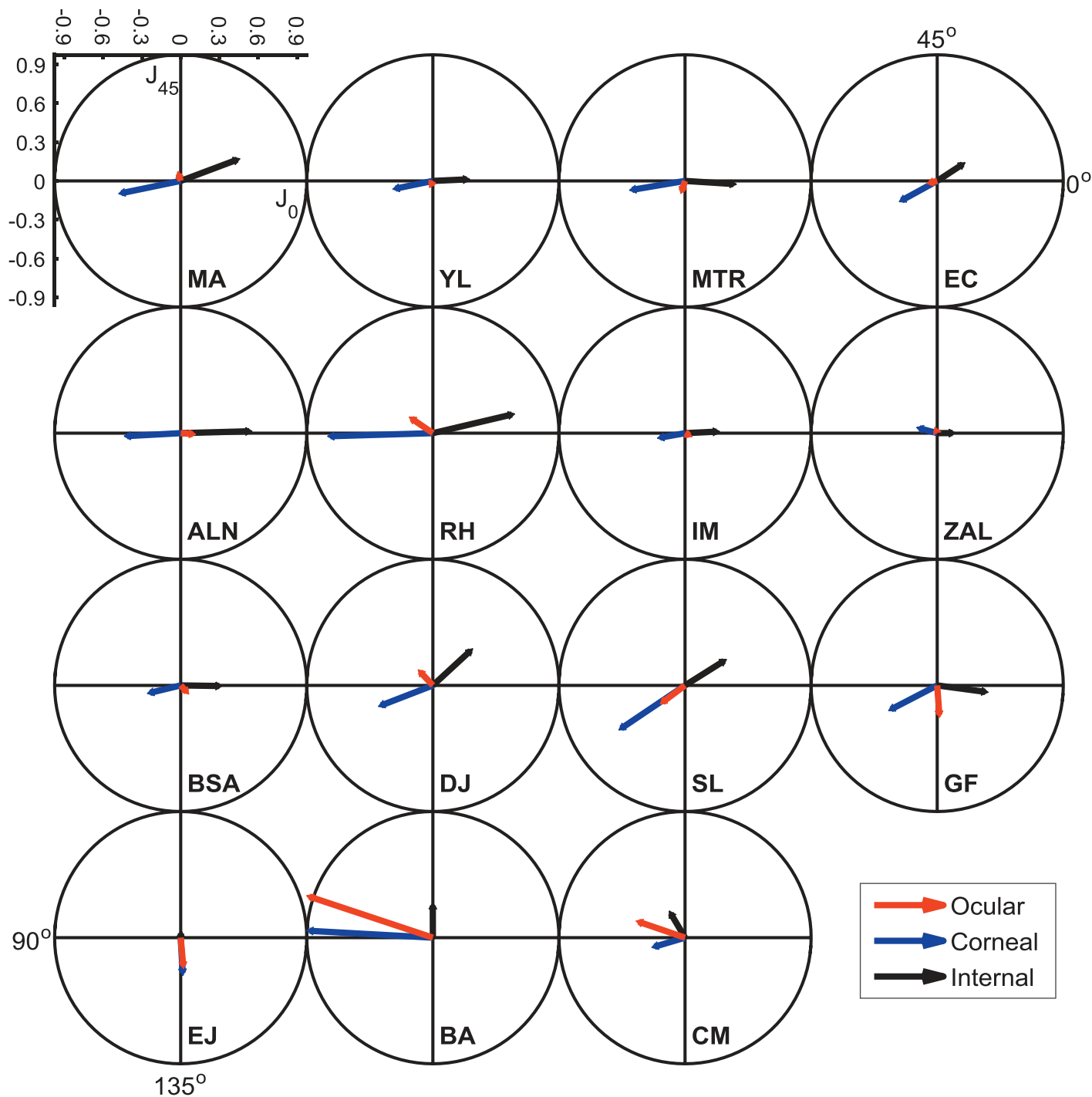
Figure 9. Population trends for the interaction of corneal and internal axial astigmatism (refers to the eye, opposite sign to clinical convention) in emmetropic eyes. Ocular (red) and internal (black) axial astigmatism averaged across eight accommodative states for individual subject are shown in corresponding subplot along with the corneal (blue) axial astigmatism. Two or three letters at the bottom of each subplot are the identifier of pertinent subject. Graphical conventions are the same as in Figure 2.

study populations of myopic and emmetropic eyes. For each eye at each accommodative state, the direction α' of the optical axis relative to the foveal LoS in object space was determined for each eye and resolved into its horizontal ($\alpha'_x =$ nasal/temporal) and vertical ($\alpha'_y =$ superior/inferior) components. The mean direction across eight accommodative states for individual eyes are represented by symbols in Figure 13 and the small horizontal and vertical lines superimposed on symbols indicate the standard errors of the mean in the corresponding directions. The relatively small extent of these error bars indicates the direction of the optical
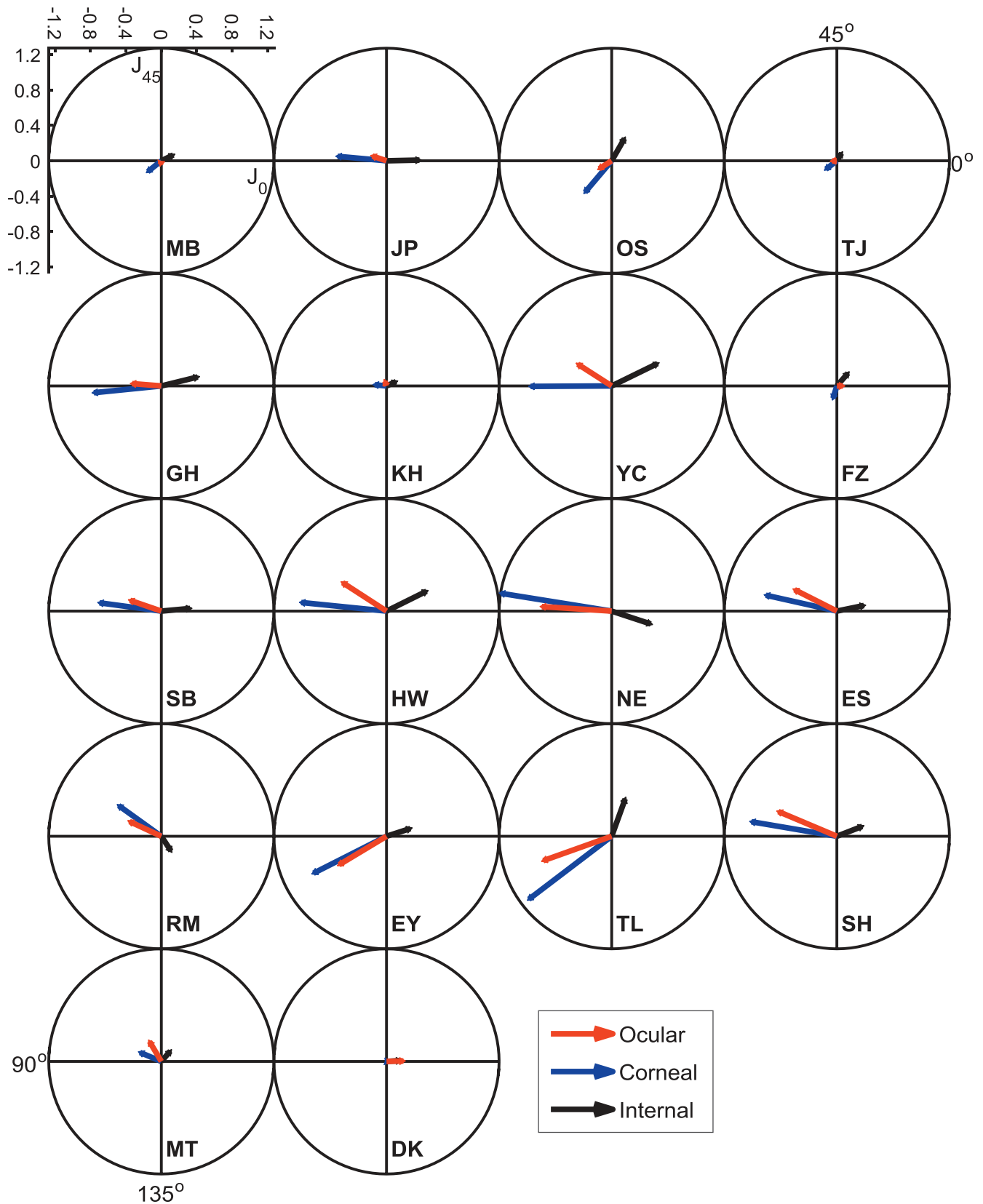
Figure 10. Population trends for the interaction of corneal and internal axial astigmatism (refers to the eye, opposite sign to clinical convention) in myopic eyes. Ocular (red) and internal (black) axial astigmatism averaged across eight accommodative states for individual subject are shown in corresponding subplot along with the corneal (blue) axial astigmatism. Two or three letters at the bottom of each subplot are the identifier of pertinent subject. Graphical conventions are the same as in Figure 2.
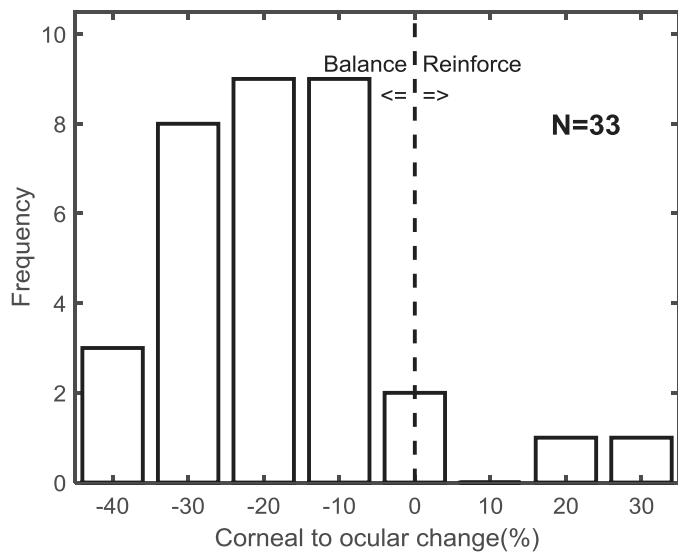
Figure 11. Frequency distribution of the computed corneal to ocular change (COC) for oblique astigmatism. COC was calculated (text Equation 6) with quadratic coefficients of ocular (averaged across eight accommodative states) and corneal oblique astigmatism in the unit of percentage for each individual, and populations combined. Positive values of COC correspond to reinforcement effect of internal optics, which causes ocular oblique astigmatism to exceed corneal oblique astigmatism. Negative values of COC correspond to a balancing effect of internal optics, which causes ocular oblique astigmatism to be less than corneal oblique astigmatism. Dashed line indicates the boundary separating reinforcement and balancing.
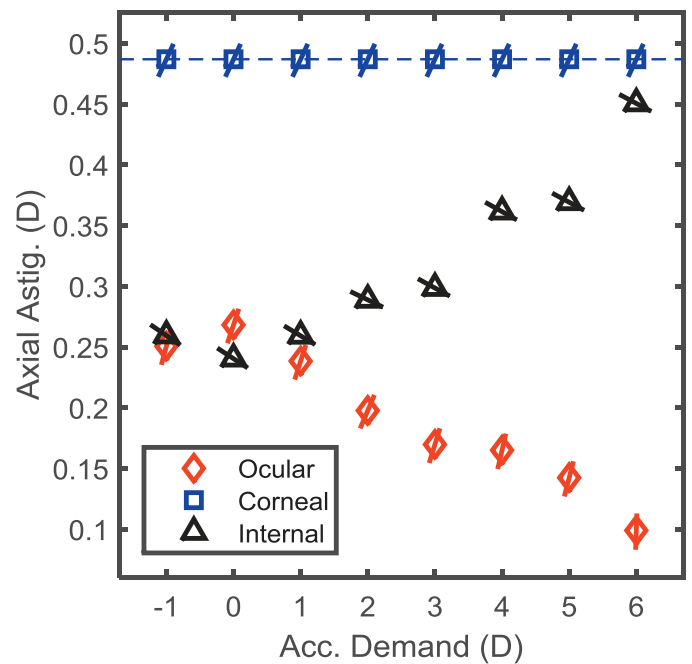

Figure 12. Example of systematic variation of axial astigmatism with accommodation for subject OS. Black and red symbols represent magnitude of internal and ocular axial astigmatism, respectively, as a function of accommodation demand. The blue dashed line and symbols indicate corneal axial astigmatism (assumed to be invariant with accommodation). The short lines through symbols show the axis of axial astigmatism, which is independent of accommodation for internal optics but when combined with corneal astigmatism causes a change in axis for total ocular astigmatism.

axis relative to the LoS is not strongly influenced by accommodation.

Except for subject GH, whose optical axis was well aligned to the LoS, the majority of optical axes were located temporally to the LoS in object space, which is consistent with our earlier observation that foveal astigmatism is a combination of axial and oblique astigmatism in most eyes. Population mean directions are shown with blue symbols in Figure 13. Mean horizontal direction for the myopic population ($\alpha'_x = -4.6°$, temporal) differed by less than 0.5° from the emmetropic mean ($\alpha'_x = -5.0°$), but the mean vertical direction for myopic eyes ($\alpha'_y = -1.6°$, superior) was nearly 3° superior to the mean for emmetropic eyes ($\alpha'_y = 1.1°$, inferior). The optical axes of individual eyes were highly concentrated about their respective population means (bias vector $|\mathbf{B}| = 0.997$ for myopic eyes and $|\mathbf{B}| = 0.999$ for emmetropic eyes), and consequently the nonzero values of the mean angle α' are statistically significant for both populations (Rayleigh test). Thus, for the purposes of defining a hypothetical average eye that represents the population mean, the present results confirm previous reports that the optical axis is about 5° away from LoS in the temporal visual field (Atchison, Smith, & Smith, 2000; Shen, Clark, Soni, &

Thibos, 2010), which suggests methodological differences in defining and locating the optical axis in previous studies and in ours are immaterial.

The pupillary axis (the corneal surface norm passing through the center of the entrance pupil) is another important reference axis that is easily located using Purkinje images (Mandell, Chiang, & Klein, 1995; Rosales & Marcos, 2007). The pupillary axis is also the corneal optical axis as defined in our study because the chief ray from an object point located on the pupillary axis would not be refracted and therefore would not suffer from oblique astigmatism. Since we located the corneal optical axis in a novel way using measurements of corneal astigmatism across the visual field, there was an opportunity to compare those results with measurements of the pupillary axis obtained by traditional methods based on biometry.

As described in the Appendix, the direction of the corneal optical axis (α'_{cx}, α'_{cy}) relative to the LoS was computed by tracing rays through customized optical models of each subject's eye constructed from the corneal astigmatism field map derived from wavefront aberrometry. An independent determination of the pupillary axis direction (λ_x, λ_y) was calculated from
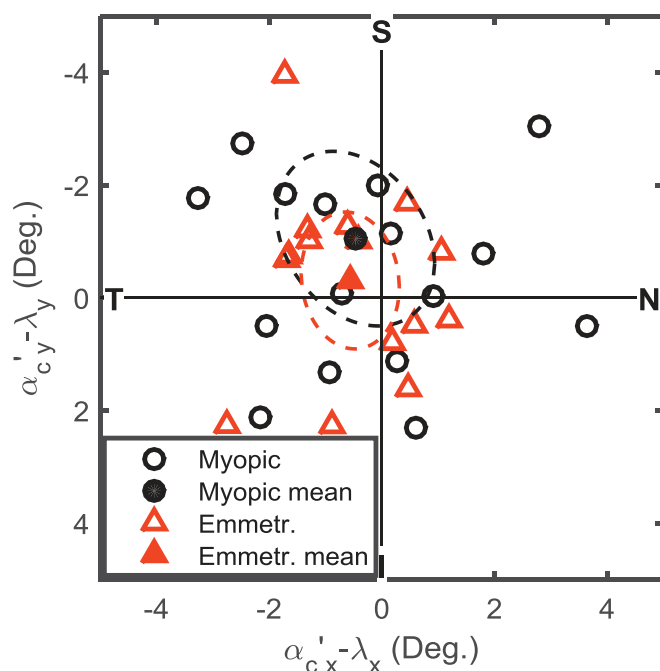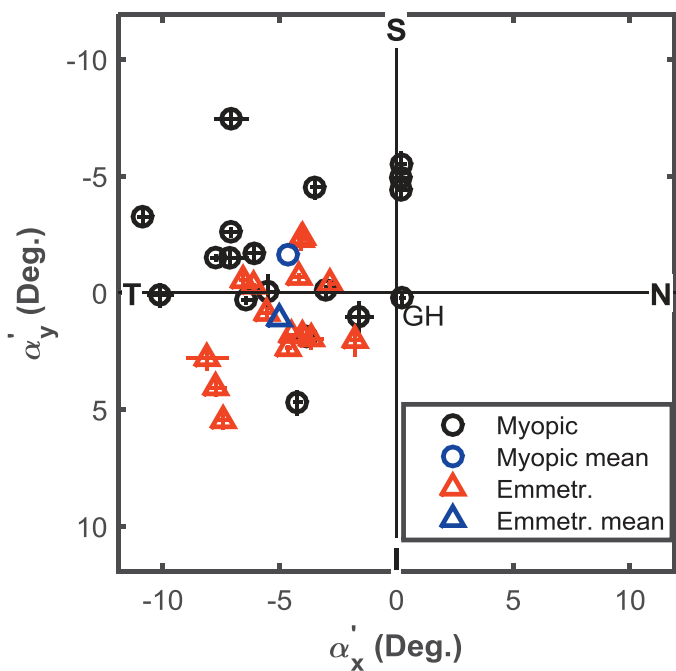
Figure 13. Comparison of distribution of angle α′ for emmetropic and myopic eyes. Axes shows the horizontal and vertical components of angle α′ in the tangent plane of Figure A1. Symbols show the mean across accommodation for individual emmetropic (red) and myopic (black). The vertical and horizontal error bars on each symbol indicate standard errors of the mean across accommodation for horizontal and vertical components of angle α′. The mean optical axis of each population is indicated by blue symbols. The origin is line-of-sight.

corneal topography data using trigonometry (see the Appendix). Since both axes are in reference to a common LoS, their mutual alignment for an individual eye is obtained by subtraction $(\alpha'_{cx} - \lambda_x, \alpha'_{cy} - \lambda_y)$, which is shown graphically in Figure 14 (top panel) as a point in a two-dimensional scatter plot. The population mean of these directional data for the emmetropic eyes and also for the myopic eyes are both within 1° of the origin. Moreover, the 95% confidence ellipses for these mean directions includes the coordinate origin, which confirms that the corneal optical axis and the pupillary axis are not significantly different (Hotelling's T^2 test $p = 0.21$ for myopic population, and $p = 0.22$ for emmetropic population). These results confirm that the pupillary axis derived from customized eye models is essentially identical to the corneal optical axis of zero oblique astigmatism. The same conclusion was reached by the two-sample version of Hotelling's T^2 test ($p = 0.56$) which confirms that oblique astigmatism of the corneal first surface is zero along the pupillary axis.

Using the same method of analysis, we may inquire whether the corneal optical axis α'_c coincides with the optical axis α' of the whole eye. Since both axes were
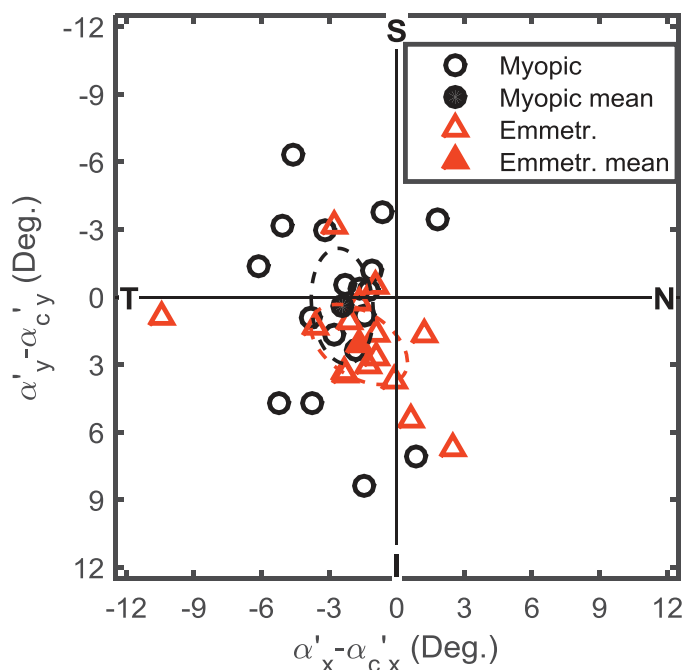

Figure 14. Comparison of ocular alignment for emmetropic and myopic eyes. Upper panel shows the misalignment $(\alpha'_c - \lambda)$ between corneal optical axis and pupillary axis for individual eyes (open symbols) and for the population mean (filled symbols). Coordinate origin is pupillary axis. Lower panel shows the misalignment $(\alpha' - \alpha'_c)$ of the angle between ocular and corneal optical axes for individual subjects (open symbols) and for the population mean (filled symbols). Coordinate origin is corneal optical axis. For both panels, dashed lines show 95% confidence ellipses for population means.

determined from aberrations and referenced to the LoS, the null hypothesis is that $\alpha' = \alpha'_c$. The distributions of these differences in direction are shown for both study populations in the bottom panel of Figure 14. Neither confidence ellipse contains the coordinate origin, which leads us to reject the null hypothesis. No significant difference was found between mean values for the two populations (Hotelling's T^2 test $p = 0.32$), so further analysis was performed on the combined populations. Mean α' for all subjects was 2.1° temporal and 1.2° inferior with respect to α'_c. This misalignment of the whole eye (α') relative to the cornea (α'_c) suggests the internal lens is tilted in the temporal direction relative to the corneal optical axis in object space, which is consistent with direct observations of lens tilt using Purkinje images (Tabernero, Benito, Alcón, & Artal, 2007).

Discussion

This report provides a comprehensive description of the source and nature of ocular astigmatism as derived from new wavefront aberrometry data obtained over the central 30° of visual field in two populations of accommodating eyes. Conceptually, ocular astigmatism has two components that depend on visual field coordinates in distinctly different ways. The axial component is due to asymmetric refracting surfaces or misaligned elements in a compound system such as the eye, and is postulated to be independent of visual field coordinates. The oblique component, on the other hand, is due to finite angles of incidence associated with off-axis object points and theoretically varies as the square of visual field eccentricity. Two anatomical sources for both of these components were identified for study. The first source is refraction by the corneal anterior surface, which is assumed to be invariant with accommodation. The second source is internal to the eye associated with the cornea's posterior surface, the crystalline lens, and wavefront propagation between cornea and lens. Novel methods were devised to quantify these axial and oblique components separately and together based on empirical measurements of astigmatism and corneal topography. Our principal finding is that accommodation has no significant impact on axial or oblique astigmatism in the central 30° of visual field, nor does accommodation affect the optical axes of the cornea, lens, or whole eye. Near the eye's optical axis, ocular astigmatism is dominated by the axial component, for which the internal source partially compensates for the corneal source. The opposite occurs at large eccentricities, where ocular astigmatism is dominated by the oblique component,
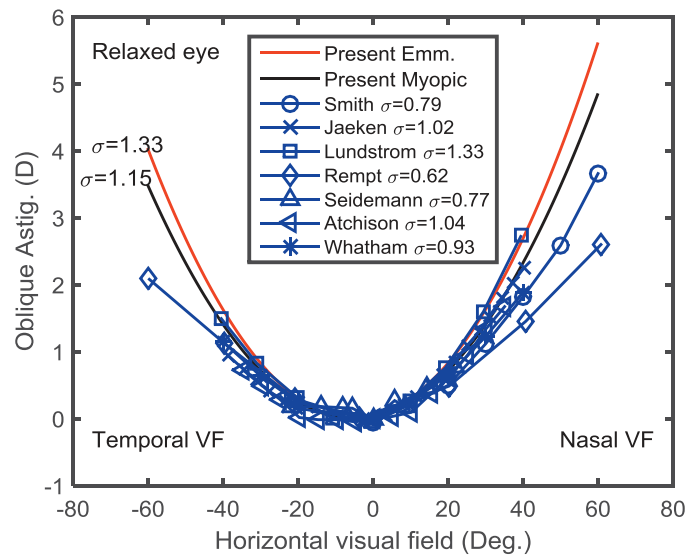

Figure 15. Comparison of the oblique astigmatism measured in this study (Black line is myopic eye, and red line is emmetropic eye) with published data (sources are denoted in the legends). For comparison, all published astigmatism measured at relaxed state along horizontal meridian were converted into power vector (only J_0 were used). The quadratic coefficients σ in 10^{-3} D/deg^2 were labeled for each population. Visual field eccentricity is marked on the abscissa with origin indicating LoS and magnitude of oblique astigmatism is shown on the ordinate.

but again the internal source compensates partially for the corneal source.

A comparison of our results with published population studies (Atchison et al., 2006; Jaeken & Artal, 2012; Lundström et al., 2009; Rempt, Hoogerheide, & Hoogenboom, 1971; Seidemann, Schaeffel, Guirao, Lopez-Gil, & Artal, 2002; Smith et al., 1988; Whatham et al., 2009) is drawn in Figure 15. Our results (red and black lines) are almost identical to prior studies using wavefront aberrometers (Jaeken & Artal, 2012; Lundström et al., 2009), but we measured higher amounts of astigmatism than studies using other techniques (photorefractor, autorefraction, refractometer, and skiascope). Regression coefficient σ of our study for the central 30° are the same order of magnitude as reported previously (mean $= 0.930 \times 10^{-3}$ D/deg^2, standard deviation $= 0.23 \times 10^{-3}$ D/deg^2). Extrapolation of our results indicated a greater degree of oblique astigmatism may be expected in the far periphery than has been reported previously.

Previous work reviewed in Introduction has revealed little effect of accommodation on ocular astigmatism either foveally or peripherally. Since ocular astigmatism for any point in the visual field is the sum of axial and oblique forms of astigmatism, it is possible that these two components change in opposite directions during accommodation, leaving their sum unaffected. Our results eliminate that possibility by showing that

axial and oblique contributions are both invariant with accommodation. Moreover, we find that axial and oblique components of corneal astigmatism are both compensated partially by internal optics across the central 30° visual field not only for the relaxed eye (Atchison, 2004; Mathur, Atchison, & Tabernero, 2012) but also for the accommodating emmetropic or myopic eye. This result, plus our observation of invariance of the optical axis, implies that any effect of accommodation on axial or lateral position of the eye's pupil has negligible effect on ocular astigmatism. The compensatory interaction of corneal and internal astigmatism affects not only magnitude but also axis. Treating astigmatism compensation as a linear sum of power vectors exposes this axis modulation, thereby providing a more complete description for individual eyes as well as population trends.

A simple way to envision lenticular shapes responsible for axial astigmatism emerges from our findings. The compensation of axial astigmatism indicates that at least one of lens surfaces is toroidal, with the meridian of minimum power meridian usually aligned with the meridian of maximum corneal power. Our finding that ocular axial astigmatism is independent of accommodation suggests that changes in zonular tension during accommodation are uniformly distributed across the lens so that the toricity of the lens is retained.

Although the difference of ocular oblique astigmatism between our two study populations is small (0.04 D at 15° eccentricity, Figure 6) and may seem functionally insignificant, the quadratic nature of oblique astigmatism predicts much larger differences for peripheral field locations beyond 15° eccentricity that might play an important role in emmetropization and myopia development. For example, at 45° eccentricity, our results predict the average emmetropic eye will exhibit 0.36 D more oblique astigmatism than the average myopic eye, which is somewhat larger than the measured value (0.26 D) reported by other researchers (Seidemann et al., 2002). If astigmatism of the peripheral field influences myopia development, then our findings suggest that increased astigmatic blur may protect emmetropic eyes from excessive growth.

Limitations of the study

In this study we calculated corneal astigmatism from surface topography of the anterior cornea. We lacked a method for measuring topography of the posterior cornea and therefore included posterior corneal aberrations in our measure of internal astigmatism. This posterior corneal contribution appears to be small, however, according to a recent empirical study (Atchison, Suheimat, Mathur, Lister, & Rozema, 2016)

reporting that the posterior cornea compensates less than 5% of anterior corneal lateral astigmatism. That conclusion agrees with our theoretical analysis (Liu & Thibos, in press) indicating the posterior cornea contributes less than 7% to the compensation of the oblique astigmatism of anterior corneal surface. Theory indicates that compensation of corneal astigmatism by internal optics is due mainly to the highly converging nature of wavefronts incident upon the lens resulting from corneal refraction (Liu & Thibos, in press).

In general, optical aberrations depend upon object distance, so the same object distance should be used when comparing aberrations of the cornea with the whole eye. We measured ocular aberrations for the same object distance used to elicit accommodation (which varied between individuals, between visual field locations, and between accommodative states), but always computed corneal first-surface aberrations for a distant object. To quantify this potential source of error, we recalculated corneal astigmatism at 15° eccentricity for all eyes using the appropriate optical conjugate determined experimentally by the refractive state (defocus) for each field position and accommodative state. Although both axial and oblique astigmatism changed systematically with object distance, the difference was less than 0.04 D of magnitude for axial and oblique astigmatism as the object moved from infinity to the near distance conjugate to the retina. We conclude that the choice of object distance had negligible impact on corneal astigmatism in our study.

We made the simplifying assumption that accommodation has no effect on corneal astigmatism. We justified this assumption with an assessment of the literature and a test case of one subject measured with and without cycloplegia. The literature is somewhat uncertain on this point, however, reporting changes in corneal shape but no change in astigmatism as the eye accommodates. We investigated this issue further by ray-tracing through a model corneal with apical radius of curvatures (7.748 mm and 7.774 mm) and conic shape factors (0.766 and 0.790) reported for far and near viewing distances, respectively (He et al., 2003). At 15° eccentricity the change of oblique astigmatism was a mere 0.005 D, which explains why the effect of shape changes during accommodation on corneal astigmatism was too small to be measured experimentally.

Another potential source of error arises from our assumption that the pupil center was at the same position during aberrometry and corneal topography. The two instruments provide different retinal illuminance, which typically caused the pupil diameter to be about 2 mm smaller in diameter during topography. This constriction might have been nonconcentric, which would have compromised our comparison of corneal and ocular aberrations. We evaluated the impact of nonconcentric pupil constriction by measur-

ing corneal topography for three subjects with natural and dilated pupils produced by cycloplegia. Cycloplegia produced more than 0.23 mm displacement of the pupil center in all three subjects, which is larger than the reported mean value (Tabernero, Atchison, & Markwell, 2009). For the worst case scenario, 0.31 mm pupil displacement introduced less than 0.066 D axial astigmatism and less than 0.009 D oblique astigmatism at 15° eccentricity.

The effect of accommodation on pupil diameter was small compared to the effect of cycloplegia. On average, accommodation reduced pupil diameter 0.7 mm in emmetropic eyes (population mean = 7.1 mm, $SD = 1.1$ mm for relaxed eyes; mean = 6.4 mm, $SD = 1.2$ mm for accommodating eyes). The average pupil constriction for the myopic population was 1.4 mm (relaxed mean = 6.9 mm, SD = 0.9; accommodating mean = 5.6 mm, SD = 1.1). These levels of pupil constriction are small compared to the constriction and concomitant decentration produced by the corneal topographer, which we argue above had negligible effect on astigmatism. We conclude, therefore, that small variations in pupil size produced by accommodation in our study would be expected to have a minor impact on nonconcentric pupil constriction and negligible impact on corneal astigmatism.

Conclusions

Despite large changes in the mean spherical component of refractive state during accommodation, the astigmatic component changes little in magnitude or axis anywhere in the central visual field. This observation greatly simplifies the task of measuring, describing, and correcting sphero-cylindrical refractive errors for extended visual objects in the accommodating eye for clinical or research purposes. Optical modeling of the accommodating eye is also simplified when refractive state is uniform across the central field (Liu et al., 2016) and the astigmatic component of refractive state is independent of accommodation. Novel methodologies developed in this study of astigmatism are appropriate also for investigating higher order aberrations, which may greatly simplify the task of modeling aberrations and retinal image quality in the accommodating eye over a large field of view.

Keywords: accommodation, axial astigmatism, oblique astigmatism, optical axis, compensation

Acknowledgments

Corresponding author: Tao Liu.
Email: liutao@indiana.edu.
Address: School of Optometry, Indiana University, Bloomington, IN, USA.

References

ANSI. (2010). American national standard Z80.28 for ophthalmics—methods for reporting optical aberrations of eyes. Merrifield, VA: American National Standards Institute.

Applegate, R. A., Thibos, L. N., Twa, M. D., & Sarver, E. J. (2009). Importance of fixation, pupil center, and reference axis in ocular wavefront sensing, videokeratography, and retinal image quality. *Journal of Cataract & Refractive Surgery*, 35(1), 139–152.

Artal, P., Benito, A., & Tabernero, J. (2006). The human eye is an example of robust optical design. *Journal of Vision*, 6(1):1, 1–7, doi:10.1167/6.1.1. [PubMed] [Article]

Artal, P., & Guirao, A. (1998). Contributions of the cornea and the lens to the aberrations of the human eye. *Optics Letters*, 23(21), 1713–1715.

Artal, P., Guirao, A., Berrio, E., & Williams, D. R. (2001). Compensation of corneal aberrations by the internal optics in the human eye. *Journal of Vision*, 1(1):1, 1–8, doi:10.1167/1.1.1. [PubMed] [Article]

Atchison, D. A. (2004). Anterior corneal and internal contributions to peripheral aberrations of human eyes. *Journal of the Optical Society of America A*, 21(3), 355–359.

Atchison, D. A., Pritchard, N., & Schmid, K. L. (2006). Peripheral refraction along the horizontal and vertical visual fields in myopia. *Vision Research*, 46(8–9), 1450–1458, doi:10.1016/j.visres.2005.10.023.

Atchison, D. A., Smith, G., & Smith, G. (2000). *Optics of the human eye* (pp. 30–38). Edinburgh: Butterworth-Heinemann.

Atchison, D. A., Suheimat, M., Mathur, A., Lister, L. J., & Rozema, J. (2016). Anterior corneal, posterior corneal, and lenticular contributions to ocular

aberrations component contributions to ocular aberrations. *Investigative Ophthalmology & Visual Science*, *57*(13), 5263–5270. [PubMed] [Article]

Beck, J. (1965). Accommodative astigmatism and pattern acuity. *Journal of the Optical Society of America*, *55*(9), 1139–1142.

Brzezinski, M. A. (1982). Review: Astigmatic accommodation (sectional accommodation)—a form of dynamic astigmatism. *The Australian Journal of Optometry*, *65*(1), 5–11, doi:10.1111/j.1444-0938.1982.tb03020.x.

Calver, R., Radhakrishnan, H., Osuobeni, E., & O'Leary, D. (2007). Peripheral refraction for distance and near vision in emmetropes and myopes. *Ophthalmic and Physiologic Optics*, *27*(6), 584–593, doi:10.1111/j.1475-1313.2007.00518.x.

Cheng, H., Barnett, J. K., Vilupuru, A. S., Marsack, J. D., Kasthurirangan, S., Applegate, R. A., & Roorda, A. (2004). A population study on changes in wave aberrations with accomodation. *Journal of Vision*, *4*(4):3, 272–280, doi:10.1167/4.4.3. [PubMed] [Article]

Davies, L. N., & Mallen, E. A. H. (2009). Influence of accommodation and refractive status on the peripheral refractive profile. *British Journal of Ophthalmology*, *93*(9), 1186–1190.

Dubbelman, M., Van der Heijde, G. L., & Weeber, H. A. (2005). Change in shape of the aging human crystalline lens with accommodation. *Vision Research*, *45*(1), 117–132, doi:10.1016/j.visres.2004.07.032.

Freeman, M., & Hasler, B. (1999). Optics (10th ed., pp. 252). London, UK: Butterworth-Heinemann.

Garner, L. F., & Smith, G. (1997). Changes in equivalent and gradient refractive index of the crystalline lens with accommodation. *Optometry & Vision Science*, *74*(2), 114–119.

Gonzalez, R. C., Woods, R. E., & Eddins, S. L. (2015). *Digital image processing using MATLAB*. New Delhi, India: McGraw Hill Education.

Harris, W. F. (2009). Optical axes of eyes and other optical systems. *Optometry & Vision Science*, *86*(5), 537–541.

He, J. C., Gwiazda, J., Thorn, F., Held, R., & Huang, W. (2003). Change in corneal shape and corneal wave-front aberrations with accommodation. *Journal of Vision*, *3*(7):1, 456–463, doi:10.1167/3.7.1. [PubMed] [Article]

Hennessy, R. T. (1975). Instrument myopia. *Journal of the Optical Society of America*, *65*(10), 1114–1120.

Jaeken, B., & Artal, P. (2012). Optical quality of emmetropic and myopic eyes in the periphery measured with high-angular resolution. *Investigative Ophthalmology & Visual Science*, *53*, 3405–3413. [PubMed] [Article]

Kelly, J. E., Mihashi, T., & Howland, H. C. (2004). Compensation of corneal horizontal/vertical astigmatism, lateral coma, and spherical aberration by internal optics of the eye. *Journal of Vision*, *4*(4):2, 262–271, doi:10.1167/4.4.2. [PubMed] [Article]

Liu, T., Sreenivasan, V., & Thibos, L. N. (2016). Uniformity of accommodation across the visual field. *Journal of Vision*, *16*(3):6, 1–16, doi:10.1167/16.3.6. [PubMed] [Article]

Liu, T., & Thibos, L. N. (2016). Interaction of axial and oblique astigmatism in theoretical and physical eye models. *Journal of the Optical Society of America A*, *33*(9), 1723–1734, doi:10.1364/JOSAA.33.001723.

Liu, T., & Thibos, L. N. (in press). Compensation of corneal oblique astigmatism by internal optics: A theoretical analysis. *Ophthalmic and Physiological Optics*, in press, doi:10.1111/opo.12364.

López-Gil, N., Martin, J., Liu, T., Bradley, A., Díaz-Muñoz, D., & Thibos, L. N. (2013). Retinal image quality during accommodation. *Ophthalmic and Physiological Optics*, *33*(4), 497–507,

Lotmar, W., & Lotmar, T. (1974). Peripheral astigmatism in the human eye: Experimental data and theoretical model predictions. *Journal of the Optical Society of America*, *64*(4), 510–513, doi:10.1364/JOSA.64.000510.

Lundström, L., Mira-Agudelo, A., & Artal, P. (2009). Peripheral optical errors and their change with accommodation differ between emmetropic and myopic eyes. *Journal of Vision*, *9*(6):17, 1–11, doi:10.1167/9.6.17. [PubMed] [Article]

Malacara, D. (2004). Handbook of optical design (2nd ed., pp. 378-380). In Z. Malacara & D. Malacara (Eds.). New York, NY: Marcel Dekker.

Mandell, R. B., Chiang, C. S., & Klein, S. A. (1995). Location of the major corneal reference points. *Optometry & Vision Science*, *72*(11), 776–784.

Mardia, K. V. (2014). *Statistics of directional data*. Academic Press. London: Academic Press.

Mathur, A., Atchison, D. A., & Charman, W. N. (2009). Effect of accommodation on peripheral ocular aberrations. *Journal of Vision*, *9*(12):20, 1–11, doi:10.1167/9.12.20. [PubMed] [Article]

Mathur, A., Atchison, D. A., & Tabernero, J. (2012). Effect of age on components of peripheral ocular aberrations. *Optometry & Vision Science*, *89*(7), 967–976.

McFadden, F. (1925). Sectional astigmia or sectional

accommodation. *American Journal of Optometry*, *2*(8), 226–230.

McKendrick, A. M., & Brennan, N. A. (1996). Distribution of astigmatism in the adult population. *Journal of the Optical Society of America A*, *13*(2), 206–214, doi:10.1364/JOSAA.13.000206.

Millodot, M. (1981). Effect of ametropia on peripheral refraction. *American Journal of Optometry and Physiological Optics*, *58*(9), 691–695.

Millodot, M. (1984). Peripheral refraction in aphakic eyes. *American Journal of Optometry and Physiological Optics*, *61*(9), 586–589.

Millodot, M., & Thibault, C. (1985). Variation of astigmatism with accommodation and its relationship with dark focus. *Ophthalmic and Physiological Optics*, *5*(3), 297–301.

Morelande, M. R., Iskander, D. R., Collins, M. J., & Franklin, R. (2002). Automatic estimation of the corneal limbus in videokeratoscopy. *IEEE Transactions on Biomedical Engineering*, *49*(12), 1617–1625.

Navarro, R., Santamaría, J., & Bescós, J. (1985). Accommodation-dependent model of the human eye with aspherics. *Journal of the Optical Society of America A*, *2*(8), 1273–1280.

Rabbetts, R. B. (2007). Bennett & Rabbetts' clinical visual optics (4th ed., pp. 208). Edinburgh, UK: Elsevier/Butterworth Heinemann.

Radhakrishnan, H., & Charman, W. N. (2007). Changes in astigmatism with accommodation. *Ophthalmic and Physiological Optics*, *27*(3), 275–280.

Rempt, F., Hoogerheide, J., & Hoogenboom, W. (1971). Peripheral retinoscopy and the skiagram. *Ophthalmologica*, *162*(1), 1–10.

Rosales, P., Dubbelman, M., Marcos, S., & van der Heijde, R. (2006). Crystalline lens radii of curvature from Purkinje and Scheimpflug imaging. *Journal of Vision*, *6*(10):5, 1057–1067, doi:10.1167/6.10.5. [PubMed] [Article]

Rosales, P., & Marcos, S. (2007). Customized computer models of eyes with intraocular lenses. *Optics Express*, *15*(5), 2204–2218.

Roselló, S., Thibos, L., & Micó, V. (2014). Step-along power vector method for astigmatic wavefront propagation. *Ophthalmic and Physiological Optics*, *34*(3), 295–308, doi:10.1111/opo.12120.

Salmon, T. O., & Thibos, L. N. (2002). Videokeratoscope–line-of-sight misalignment and its effect on measurements of corneal and internal ocular aberrations. *Journal of the Optical Society of America A*, *19*(4), 657–669.

Schwiegerling, J., Greivenkamp, J. E., & Miller, J. M. (1995). Representation of videokeratoscopic height data with Zernike polynomials. *Journal of the Optical Society of America A*, *12*(10), 2105–2113.

Seidemann, A., Schaeffel, F., Guirao, A., Lopez-Gil, N., & Artal, P. (2002). Peripheral refractive errors in myopic, emmetropic, and hyperopic young subjects. *Journal of the Optical Society of America A*, *19*(12), 2363–2373, doi:10.1364/JOSAA.19.002363.

Shen, J., Clark, C. A., Soni, P. S., & Thibos, L. N. (2010). Peripheral refraction with and without contact lens correction. *Optometry & Vision Science*, *87*(9), 642–655.

Smith, G., Millodot, M., & McBrien, N. (1988). The effect of accommodation on oblique astigmatism and field curvature of the human eye. *Clinical and Experimental Optometry*, *71*(4), 119–125.

Suheimat, M., Verkicharla, P. K., Mallen, E. A. H., Rozema, J. J., & Atchison, D. A. (2015). Refractive indices used by the Haag-Streit Lenstar to calculate axial biometric dimensions. *Ophthalmic and Physiological Optics*, *35*(1), 90–96, doi:10.1111/opo.12182.

Tabernero, J., Atchison, D. A., & Markwell, E. L. (2009). Aberrations and pupil location under corneal topography and Hartmann-Shack illumination conditions. *Investigative Ophthalmology & Visual Science*, *50*(4), 1964–1970. [PubMed] [Article]

Tabernero, J., Benito, A., Alcón, E., & Artal, P. (2007). Mechanism of compensation of aberrations in the human eye. *Journal of the Optical Society of America A*, *24*(10), 3274–3283, doi:10.1364/JOSAA.24.003274.

Thibos, L. N., Wheeler, W., & Horner, D. (1997). Power vectors: An application of Fourier analysis to the description and statistical analysis of refractive error. *Optometry & Vision Science*, *74*(6), 367–375.

Ukai, K., & Ichihashi, Y. (1991). Changes in ocular astigmatism over the whole range of accommodation. *Optometry & Vision Science*, *68*(10), 813–818.

Vazquez, D., Acosta, E., Smith, G., & Garner, L. (2006). Tomographic method for measurement of the gradient refractive index of the crystalline lens. II. The rotationally symmetrical lens. *Journal of the Optical Society of America A*, *23*(10), 2551–2565, doi:10.1364/JOSAA.23.002551.

Wei, X., & Thibos, L. (2010a). Design and validation of a scanning Shack Hartmann aberrometer for measurements of the eye over a wide field of view. *Optics Express*, *18*(2), 1134–1143.

Wei, X., & Thibos, L. N. (2010b). Modal estimation of wavefront phase from slopes over elliptical pupils. *Optometry & Vision Science*, *87*(10), 767–777.

Welford, W. T. (1986). *Aberrations of optical systems*. Bristol, England: CRC Press.

Whatham, A., Zimmermann, F., Martinez, A., Delgado, S., de la Jara, P. L., Sankaridurg, P., & Ho, A. (2009). Influence of accommodation on off-axis refractive errors in myopic eyes. *Journal of Vision*, *9*(3):14, 1–13, doi:10.1167/9.3.14. [PubMed] [Article]

Appendix: Conventions for displaying visual field maps of astigmatism

Aberration data are displayed as visual field maps using the coordinate system illustrated in Figure A1. The foveal LoS in object space defines a *z* axis that is perpendicular to a tangent plane for specifying test locations in Cartesian (*x*, *y*) or in polar (eccentricity, ε and meridian, θ) coordinates. The line joining a test point with the center of the left eye's entrance pupil can be regarded as a peripheral LoS that coincides with the corresponding measurement axis (MA) of the scanning

aberrometer. For graphical purposes in this report, visual field maps are oriented and labeled as if seen by the subject's left eye (and also the reader's left eye), with the top of the map occupying the superior field and the left side occupying the temporal field. Mathematical coordinates of the field maps are specified in Cartesian (*x*, *y*) form with positive *x* values indicating nasal visual field and positive *y* values indicating inferior field. The same maps can also be interpreted in retinal coordinates, in which case positive *x* values indicate temporal retina and positive *y* values indicate superior retina for the location of the image of the test spot, which acts as a retinal beacon reflecting light out of the eye for measurement by the aberrometer.

Iterative method for locating the optical axis

Our iterative method for locating the optical axis from visual field maps of ocular astigmatism is illustrated in Figure A2 with simulated data from a rotationally symmetric schematic eye with the optical axis displaced 3° by a known amount horizontally and 5° vertically with respect to the foveal line-of-sight. Black dots indicate the measured field locations, one of which is labeled P. The oriented black line through each dot is parallel to the axis of astigmatism and the line's length indicates astigmatism magnitude. If extended,
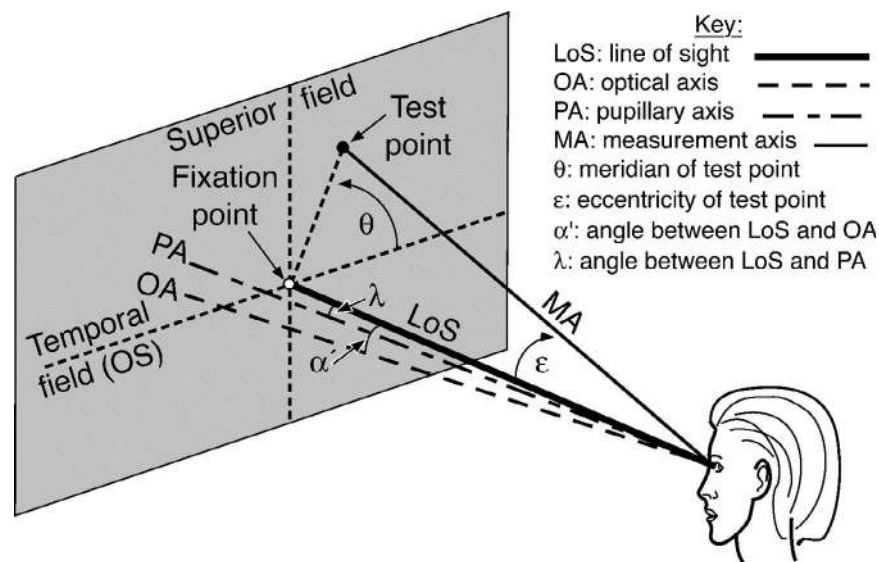

Figure A1. Reference axes and visual field coordinates in object space for left eye. Line of sight (LoS) is the line passing through fixation point and entrance pupil center. Optical axis (OA) is defined as the line passing through the entrance pupil center along which oblique astigmatism is zero. Pupillary axis (PA) is that anterior surface norm of the cornea which passes through the entrance pupil center. Measurement axis (MA) of the aberrometer coincides with the chief ray from a test point on the tangent screen. The tangent screen is orthogonal to LoS at the fixation point. The probe beam of ISAW is injected along MA and reflected light is analyzed for wavefront aberrations relative to MA. Visual field locations may be specified in polar angular coordinates as eccentricity ε and meridian θ or in Cartesian coordinates by the *x*, *y* coordinates of the tangent screen (LoS is the *z* axis). The angle between LoS and OA is α', which has horizontal and vertical components α'_x, α'_y. The angle between LoS and PA is λ with components λ_x, λ_y.
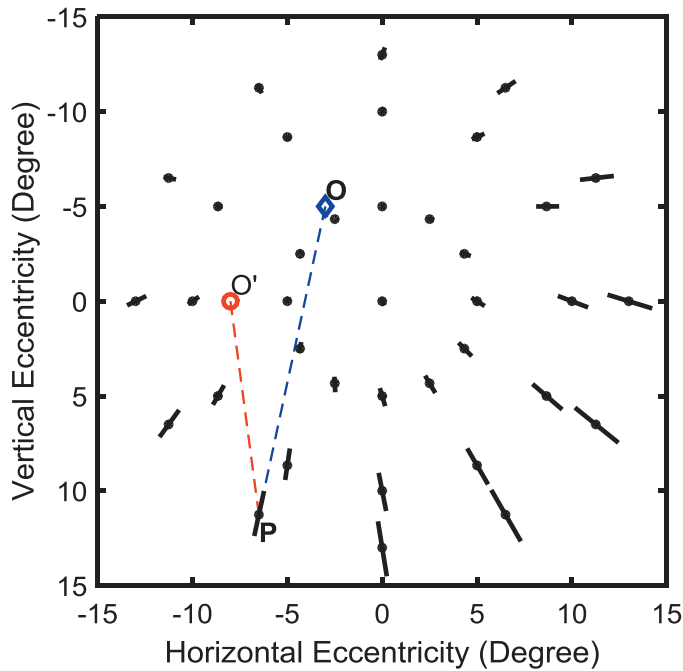
Figure A2. Iterative method for locating the optical axis, illustrated with simulated data from a rotationally symmetric schematic eye with optical axis displaced 3° horizontally and 5° vertically with respect to line-of-sight. Black dots indicate the measured field locations, one example of which is labeled P. Oriented black line through each dot is parallel to the axis of astigmatism and the line's length indicates astigmatism magnitude. (If extended, the oriented lines all intersect at the optical axis location for this symmetric eye model, but in general do not.) The model's optical axis intersects the tangent screen at the blue diamond labeled O, which is connected to test point P by a vector (blue dashed line). A candidate location for the optical axis is shown by the red circle labeled O′, which is connected to the test point P by the red dashed line. For each test location, the astigmatism vector is projected onto the corresponding red line and the scalar sum of these projected lengths for all field locations is computed. Using an iterative algorithm, the candidate location O′ moves around the visual field until this sum of projections is maximized. In principle, this maximum location is O, the optical axis, because the axis of oblique astigmatism is always radial and therefore produces the largest possible projection for every field location.

the oriented lines would all intersect at the optical axis location for this symmetric eye model; but for eyes with axial astigmatism, they do not intersect. The model's optical axis intersects the tangent screen at the blue diamond labeled *O*, which is connected to test point *P* by a vector (blue dashed line). A candidate location for the optical axis is shown by the red circle labeled *O′*, which is connected to the test point *P* by the red dashed line. For each test location, the astigmatism vector is projected onto the corresponding red line and the scalar sum of these projected lengths for all field locations is

computed. Using an iterative algorithm, the candidate location *O′* moves around the visual field until this sum of projections is maximized. In principle, this maximum location is *O*, the optical axis, because the axis of oblique astigmatism is always radial and therefore produces the largest possible radial projection for every field location. The method works best when axial astigmatism is weak or absent, so the maps were preconditioned by subtracting the average across all states of accommodation of the space average value of astigmatism across visual field.

Correction of corneal topography for misalignment of VK axis relative to LoS

Corneal topography measurements are referenced to the vertex normal (VK axis), while ocular aberrations are referenced to the LoS. Usually these two reference axes do not coincide, which can introduce errors when comparing corneal and ocular aberration (Applegate et al., 2009; Salmon & Thibos, 2002). To avoid this potential problem, corneal surface topography referenced to the VK axis was mathematically transferred (by translation plus rotation) to the LoS before computing corneal aberrations. To perform this correction required knowledge of the location of the pupil relative to the cornea in three-dimensional space. A common approach is to independently measure angle λ between LoS and pupillary axis and then calculate tilt and decentration of the cornea relative to LoS (Atchison, 2004; Rosales & Marcos, 2007; Salmon & Thibos, 2002). Instead, we developed the following geometrical method to locate the pupil center relative to the cornea using the spatial relationships shown in the Appendix, Figure A3.

To facilitate pupil edge detection based on the intensity gradient at the edge of the pupil (Morelande, Iskander, Collins, & Franklin, 2002), the overlaid Placido rings were removed with two morphological operations, opening and closing (Gonzalez, Woods, & Eddins, 2015), and the results were verified by visual inspection. The angular as well as the lateral misalignment between VK axis and LoS could be determined from the known distance between fixation target and cornea, anterior chamber depth (from Lenstar biometry), radius of curvature of cornea (from topography), and pupil shift relative to corneal reflex (from topography raw images) as follows. With reference to Figure A3, the decentration and tilt of the VK axis relative to LoS are given by SV and angle θ, respectively. FV = 59.7 mm. ED was estimated with the deviation of entrance pupil center (E) from center of Placido rings (D) in videokeratoscopic images. The entrance pupil depth VD could be computed from measured anterior chamber depth VL by considering
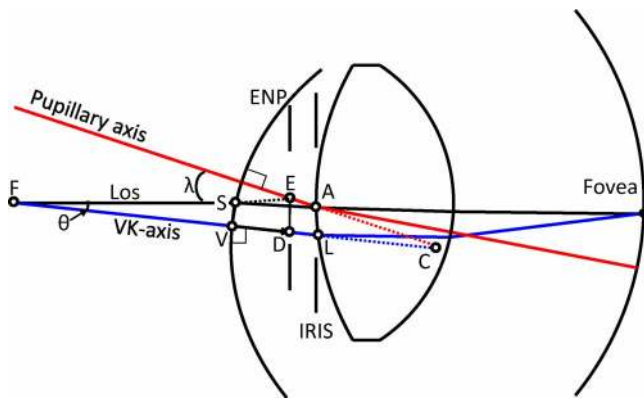
Figure A3. Geometry used to calculate the misalignment of the cornea and pupillary axis relative to LoS based on corneal topography measurement. The posterior corneal surface is ignored here, and anterior cornea is assumed to be spherical. All the solid lines are real optical paths with refraction taken into account, and the dotted lines are extensions. The VK axis is FVDLC, where F is the fixation target of corneal topographer, V is the corneal vertex, D and L are intersections of VK at entrance pupil and iris plane respectively, and C is the center of curvature of the anterior cornea (best-fit sphere) in the neighborhood of V. The LoS is FSE, where S is the corneal sighting center, and E is the entrance pupil center. The pupillary axis is EAC, where A is the iris center.

refraction by the cornea and assuming refractive index 1.3375,

$$VD = 1/(1.3375/VL - 0.3375c_m),$$

where c_m is the mean power of anterior cornea reported by topographer.

The tilt and decentration of the cornea are then given by

$$\theta = \tan^{-1}[ED/(FV + VD)]$$

$$SV = \tan\theta \times FV.$$

In triangle *EDC*,

$$\angle ECD = \tan^{-1}[ED/(VC - VD)],$$
    where $VC = 1/c_m$.

In triangle *EFC*,

$$\lambda = \theta + \angle ECD.$$

We computed corneal aberrations from corrected topographic data using an individualized corneal model implemented with the optical design software program Zemax OpticStudio (Zemax, LLC, Kirkland, WA) as follows. The z axis was aligned with the LoS, the anterior corneal surface sag was represented by Equation 3, tilted and decentered appropriately, the

stop aperture (physical pupil) was placed at the position determined by anterior chamber depth measurements. The entrance pupil was set equal to the minimum pupil size during ocular aberration measurements, and the object was placed at infinity. The posterior cornea was ignored and refractive index of image space was set equal to 1.3700 as predicted by chromatic dispersion (Navarro, Santamaría, & Bescós, 1985) of the cornea at 850 nm. The model's imaging surface (i.e., model retina) was a sphere with 12 mm radius of curvature positioned to eliminate paraxial focusing errors along the foveal LoS. Then the numerical ray tracing was performed along the same scanning pattern carried out in our ocular aberration experiment. The resultant Zernike coefficients for corneal aberrations were scaled appropriately to match the eye's pupil size during ocular aberration measurements (which varied with accommodation), and the results expressed as power vectors for corneal astigmatism as described previously (Liu & Thibos, 2016).

Directional data analysis

Statistics of axis direction and orientation were computed using the methods of directional data analysis (Mardia, 2014). For example, the direction of the optical axis relative to the foveal LoS are specified initially in polar coordinates by eccentricity and meridian (ε, θ) but then are transformed into directional cosines for computing statistics (see chapter 8 of Mardia, 2014). The resulting mean direction was then projected back onto the tangent plane for display.

Directional data methods were also used on astigmatism data specified in power vector form. Power vectors represent astigmatism by a two-dimensional vector **J** with a magnitude and direction equal to twice the axis angle. To compute the mean of N power vectors we divide their vector sum by N, $\bar{\mathbf{J}} = \sum_{i=1}^{N} \mathbf{J}/N$. This mean power vector might be used to specify trends in astigmatism axis but is sensitive to absolute magnitudes of astigmatism. This problem is avoided by normalizing the mean astigmatism vector by the average length of the vectors $\sum_{i=1}^{N}|\mathbf{J}|/N$. The result is a bias vector $\mathbf{B} = \sum_{i=1}^{N} \mathbf{J}/\sum_{i=1}^{N}|\mathbf{J}|$ which has the following interpretation: The angle of the bias vector is the mean direction (i.e., central tendency) of the population, and the length of the bias vector is the concentration of the directional data about the mean direction on an absolute scale of 0 (random directions) to 1.0 (all directions the same). Since power vectors exist in a double-angle space, the mean direction must be divided by 2 for interpretation as the mean axis of astigmatism.